The regional distribution of zeolites in the basalts of the Faroe Islands and the significance of zeolites as palaeotemperature indicators

Ole Jørgensen

The first maps of the regional distribution of zeolites in the Palaeogene basalt plateau of the Faroe Islands are presented. The zeolite zones (thomsonite-chabazite, analcite, mesolite, stilbite-heulandite, laumontite) continue below sea level and reach a depth of 2200 m in the Lopra-1/1A well. Below this level, a high temperature zone occurs characterised by prehnite and pumpellyite. The stilbite-heulandite zone is the dominant mineral zone on the northern island, Vágar, the analcite and mesolite zones are the dominant ones on the southern islands of Sandoy and Suðuroy and the thomsonite-chabazite zone is dominant on the two northeastern islands of Viðoy and Borðoy. It is estimated that zeolitisation of the basalts took place at temperatures between about 40°C and 230°C. Palaeogeothermal gradients are estimated to have been 66 ± 9°C/km in the lower basalt formation of the Lopra area of Suðuroy, the southernmost island, 63 ± 8°C/km in the middle basalt formation on the northernmost island of Vágar and 56 ± 7°C/km in the upper basalt formation on the central island of Sandoy.

A linear extrapolation of the gradient from the Lopra area places the palaeosurface of the basalt plateau near to the top of the lower basalt formation. On Vágar, the palaeosurface was somewhere between 1700 m and 2020 m above the lower formation while the palaeosurface on Sandoy was between 1550 m and 1924 m above the base of the upper formation.

The overall distribution of zeolites reflects primarily variations in the maximum depth of burial of the basalt rather than differences in heat flow. The inferred thinning of the middle and upper basalt formation from the central to the southern part of the Faroes is in general agreement with a northerly source area for these basalts, centred around the rift between the Faroes and Greenland. The regional zeolite distribution pattern is affected by local perturbations of the mineral zone boundaries that reflect local differences in the temperature, perhaps related to the circulation of water in the underground. The zonal distribution pattern suggests that these temperature anomalies are in part related to NW–SE-trending eruption fissures or zones of weakness separating the present islands and are subparallel to transfer zones in the Faroe–Shetland Basin. Both the regional and the local distribution of zeolite assemblages are probably a reflection of the basic volcanic-tectonic pattern of the Faroe Islands.

Keywords: Faroe Islands, Palaeogene basalt plateau, zeolite zone, palaeotemperature indicators

O.J., *Scandinavian Asbestos & Mineral Analysis, Kildeskovsvej 62, DK-2820 Gentofte, Denmark.* E-mail: *Oj@oj-sama.dk*

The zeolites of the Faroe Islands have been known for more than 300 years (Debes 1673) although the islands remained nearly unknown to mineralogists until the end of the eighteenth century. Because of increasing interest in mineralogy in the nineteenth century, the Faroe Islands were visited by many naturalists. One of these was Brewster (1825), who proposed the name levyne for a new zeolite species he discovered at Dalsnípa on Sandoy. The first modern description of the distribution of Faroese minerals was published by Currie (1905), who visited the Faroe Islands and described the minerals at 120 localities. Five years later a new description of the Faroese zeolites was presented by Görgey (1910). Interest in the minerals of the Faroe Islands declined during the following 70 years until Betz (1981) visited the islands and reviewed the classic localities. The present author started a literature study to discover, if a system of zeolite zones exists on the Faroe Islands similar to that described by Walker (1960) in East Iceland, but concluded that published descriptions were based on minerals from the same set of localities that were known to be rich in mineral species and where large crystals could be collected. This sampling bias meant that it was not possible to decide if zeolite zones existed on the Faroe Islands, so in 1979 a systematic mapping of the zeolites in the Faroe Islands was initiated by the present author. During the following 20 years, more than 800 localities were visited and about 3000 rock samples were investigated in the field and in the laboratory. The work was extended by studying samples from the Vestmanna-1 and Lopra-1 boreholes drilled in 1980 and 1981, respectively (Jørgensen 1984; Waagstein *et al.* 1984). In 1996, the Lopra-1 borehole was deepened to a total of 3565 m (Lopra-1/1A) and the secondary minerals in the deepened part of the Lopra well were also described by the present author (Jørgensen 1997).

The aim of the present paper is to describe the secondary mineral distribution in the exposed parts of the Faroe Islands and in the Lopra-1/1A and Vestmanna-1 wells. The results of the mapping are used to estimate the palaeogeothermal gradients and the altitudes of the palaeosurfaces at various places in the Faroes basalt succession. The following topics will be discussed: (1) the general conditions for the use of zeolites as palaeotemperature indicators and the statistical distribution of zeolites in a vertical profile, (2) the original thickness of the three basalt formations and the volcanic evolution of the Faroese basalt complex, and (3) the regional distribution of the zeolite zones as a function of the thicknesses of the middle and the upper basalt formations.

Outline of the geology of the Faroe Islands

The Faroe Islands (62°N, 7°W) have a total area of 1400 km^2, an average height of 300 m above sea level and form part of the North Atlantic Brito-Arctic Cenozoic Igneous Province that extends from the British Isles to Greenland. The Faroe Islands consist almost exclusively of flood basalts that were erupted about 59–55 Ma (Waagstein 1988; Larsen *et al.* 1999).

The basalts on the exposed part of the Faroe Islands are divided into a *lower*, a *middle* and an *upper basalt formation*, separated by two horizons termed A and C in Fig. 1 (see also Fig. 4). According to Rasmussen & Noe-Nygaard (1969, 1970) the volcanic evolution of the Faroe Islands may be summarised as follows: Volcanic activity started west of the present islands with the eruption of the *lower basalt formation*. With time the production rate of lava slowed to a temporary standstill. During this quiet period, about 10 m of clay and coal bearing sediments were deposited (the *A-horizon.*). Volcanic activity restarted with an explosive phase, resulting in the deposition of coarse volcanic ash and agglomerates. An effusive phase followed during which the *middle basalt formation* was erupted from
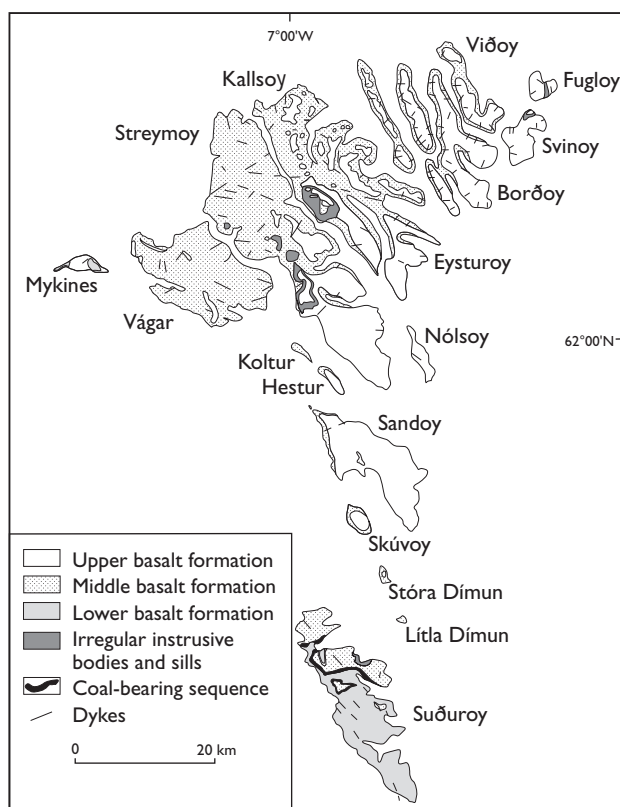

Fig. 1. Geological map of the Faroe Islands. From Rasmussen & Noe-Nygaard (1969).

several vents and small fissures within the present group of islands. Finally, volcanic activity moved farther east, away from the present islands, causing the lava flows of the *upper basalt formation* to transgress the middle basalt formation from the east. The discordant surface between the middle and upper basalt formations is named the *C-horizon*. After the upper basalt formation was formed, the basalt plateau was intruded by dykes and sills. Large sills were intruded near the boundary between middle and upper basalt formations in Streymoy and Eysturoy. Tectonic activity continued long after the volcanism ended until the Faroese basalt pile acquired its present gentle easterly dip.

Methodology

Sampling and mineral identification

Renewal of a large part of the road system of the Faroes just before initiation of the fieldwork made it possible to collect samples in fresh road cuts and new quarries along the roads. After most of the road sites had been examined, the mountains were traversed and samples collected along the old paths between the villages. In addition to the samples collected by the author, the present investigation is based on 500 specimens of Faroese zeolites collected privately by K. Jørgensen and on the collection of Faroese zeolites in the Geological Museum, Copenhagen.

The minerals were identified by their crystal morphology, optical properties, and X-Ray Diffraction (XRD) patterns or by chemical analysis carried out on a scanning electron microscope equipped with an energy dispersive analytical system. The XRD reference patterns were taken from Gottardi & Galli (1985).

Mapping of the mineral zones

Walker (1960, 1970) defined his zeolite zones by seven distinctive amygdale mineral assemblages. Each zone was

Table 1. Abbreviations used for mineral names

An: analcite	Le: levyne
Ap: apophyllite	Me: mesolite: solid
Ca: calcite	Me*: mesolite: hair-like
Ce: celadonite	Mo: mordenite
Ch: chabasite	Na: natrolite
Cl: chlorite	Ok: okemite
Cld: chalcedony	Op: opal
Ed: epidote	Ph: phillipsite
Ep: epistilbite	Pr: prehnite
Ga: garronite	Pu: pumpellyite
Gi: gismondine	Qz: quartz
Gy: gyrolite	Sc: scolecite
Ha: harmotom	Sm: smectites
He: heulandite	St*: stellerite
La: laumontite	

Mineral zones	Approx. temperatures in °C †	Ch	Th*	Th	An	Me*	Ph	Le	Me	Gy	Mo	St	He	Ep	Ap	La	Pr	Pu	Ed	Cl	Ce	Sm	Qz	Cld	Op	Ca
0 Zeolite free zone	40–60																									
1 Chabazite-thomsonite	50–70																									
2 Analcite																										
3 Mesolite	90–100																									
4 Stilbite-heullandite	110–130																									
5 Laumontite	190–230																									
6 High temperature zone	> 300																									

† Source: Kristmannsdóttir & Tómasson (1978), Kristmannsdóttir (1982) and Jakobsson & Moore (1986)

Fig. 2. Mineral temperature scale. The five zeolite zones are defined by the index minerals chabasite + thomsonite, analcite, mesolite, stilbite + heulandite and laumontite. The temperatures are shown at zone boundaries. Abbreviations used for the various minerals are shown in Table 1.

defined by the presence or dominance of certain mineral species, termed index minerals, whose names are used to designate the zones. In addition to the index minerals, other minerals may be present as indicated in Fig. 2. Walker's (1960) original zones are the carbonate, chabazite-thomsonite, analcite, mesolite, laumontite, prehnite and epidote zones. The original mesolite zone was later subdivided into a mesolite and a stilbite-heulandite zone. This extended zone definition was adopted in the present investigation (Fig. 2). The classification of the zeolite zones was normally based on the mineral assemblages of amygdales, and fracture fillings were used only in places without amygdales.

Classification of the mineral assemblages from samples from the Lopra-1/1A and Vestmanna-1 boreholes was originally based on the abundance of the individual index minerals expressed as the weight% of the total mass of index minerals (Jørgensen 1984). In the present investigation, which is based on about 3000 samples, quantitative analysis was carried out only on two selected mineral assemblages, one from the middle and one from the upper basalt formation. The assemblages from most localities consist of a large number of minerals which makes it difficult to estimate the relative abundance of the different minerals. Another complication was the fact that more than one index mineral often occurred at the same locality. The present investigation is therefore based on the *first formed index minerals in the amygdales,* i.e. the minerals that were deposited nearest to the host rock. Where more than one first formed index mineral was present at a locality, the index mineral assumed to have the highest temperature of formation was chosen to map the zones. The mineral zones mapped in this way thus reflect *the maximum temperature of mineralisation.* This method is different from a mapping based on abundance of the minerals, which shows the distribution of the zeolite zones as the result of the main mineralisation. Appendices A and B give the observed paragenesis in the 29 sections and two

Table 2. Relative frequency (in %) of amygdales and mineralised fractures in the exposed part of the Faroe Islands

Mineral	Average	Suðuroy	Sandoy	Vágar	Streymoy	Eysturoy	Borðoy	Viðoy
Zeolites:								
Analcite	*32*	**61**	*16*	*49*	*33*	*35*	*18*	*15*
Chabazite	**67**	**61**	*65*	*71*	*78*	*76*	*62*	**66**
Cowlesite	1	7	0	0	0	2	0	0
Epistilbite	<1	0	0	3	0	0	0	0
Garronite	4	8	0	6	8	8	0	0
Gismondine	4	0	10	0	5	8	3	0
Heulandite	*30*	*51*	**69**	*77*	*60*	*63*	*38*	*38*
Laumontite	11	5	*6*	*29*	*29*	3	5	0
Levyne	*17*	5	*16*	*23*	*20*	*26*	8	*20*
Mesolite	**61**	*56*	*65*	*86*	*63*	*60*	*48*	*50*
Mordenite	8	*12*	0	*14*	8	*19*	0	0
Natrolite	4	*10*	0	9	0	5	3	0
Scolecite	1	2	0	0	0	3	0	0
Stellerite	*45*	*24*	*55*	*26*	*20*	13	6	9
Stilbite	*37*	*37*	10	**74**	*38*	*39*	*33*	*26*
Phillipsite	8	*17*	6	*3*	*3*	11	10	15
Thomsonite	**64**	*59*	*45*	**60**	*60*	*75*	*73*	**79**
Other minerals:								
Apophyllite	*15*	*12*	*13*	*29*	*20*	*27*	3	*0*
Calcite	*36*	*37*	*39*	*34*	*43*	*32*	*32*	*32*
Celadonite	*19*	*15*	*13*	11	*38*	*27*	14	*15*
Chlorite	8	*10*	3	3	*23*	13	5	
CSH	2	5	0	3	0	8	0	15
Gyrolite	12	7	3	*14*	*28*	*29*	0	*21*
Smectites	*18*	7	3	*36*	*23*	*26*	16	
Silica minerals	*19*	*29*	6	*14*	*20*	*19*	*25*	41
Visited localities		160	85	148	302	235	52	41

Abundant minerals in **bold face**, common minerals in *italics* and rare minerals in normal type face. CSH is calcium silicate hydrates. Silica minerals are opal, chalcedony etc.
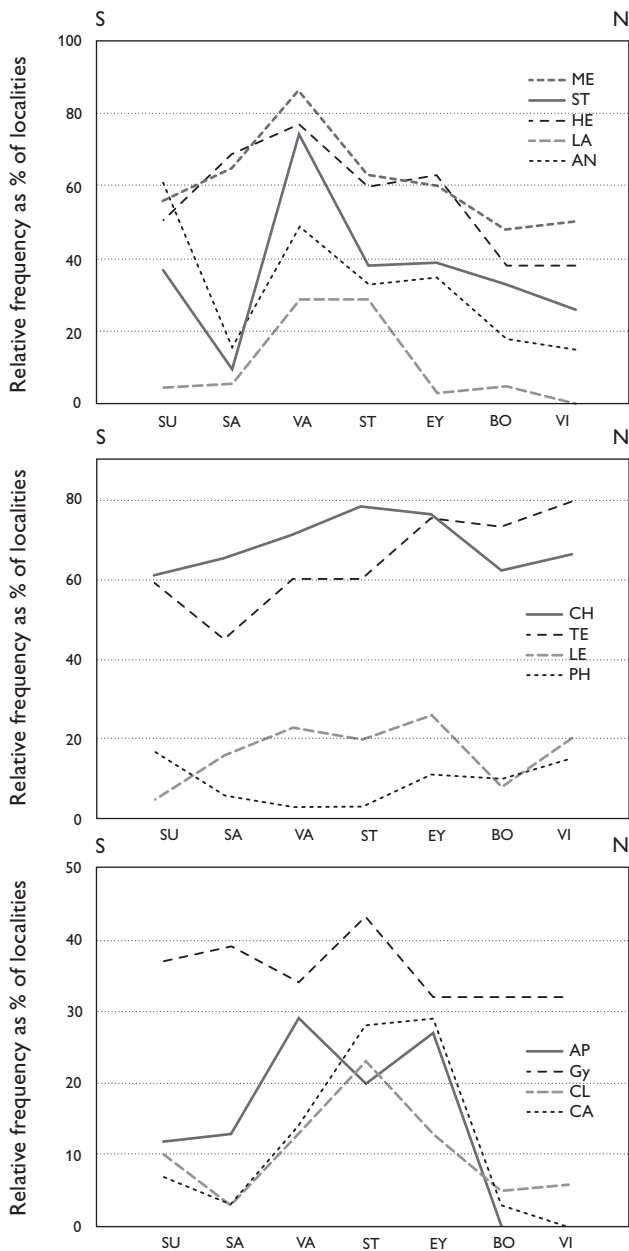
Fig. 3. Variation diagrams of the relative frequency of minerals on Suðuroy (SU), Sandoy (SA), Vágar (VÁ), Streymoy (ST), Eysturoy (EY), Borðoy (BO) and Viðoy (VI). Contractions for zeolite names are listed in Table 1.

be determined only when part of the host rock adhered to the sample.

In order to establish a correlation between the zeolite zones and the temperature of formation of the minerals, the vertical distribution of index minerals and temperatures was examined in a number of boreholes in the geothermal areas of Iceland (Kristmannsdóttir & Tómasson 1978; Kristmannsdóttir 1982). The result was the mineral–temperature scale shown in Fig. 2. Examination showed that the temperatures at the boundaries of individual zeolite zones varied from place to place. This is probably caused by the fact that zeolites can be formed within a broad range of temperatures and that variations in the chemical composition of the rock and the hydrothermal solutions can affect the formation temperature of the zeolites (Barth-Wirsching & Höller 1989; Breck 1974). Another problem that makes it difficult to determine accurately the palaeotemperatures at the zone boundaries is the fact that zone boundaries are not well defined lines, a problem that will be discussed below. The temperatures at the boundaries of the zeolite zones are therefore indicated in Fig. 2 at the lowest and highest temperatures that occur at the Icelandic zone boundaries.

As mentioned above, the original classification of the mineral assemblages of the Lopra-1/1A and Vestmanna-1 drillholes was based on the most abundant index zeolite. It was therefore necessary to re-classify the mineral assemblages of the two drillholes according to the method used in the present investigation. This had a rather small effect on the zonation of the Lopra-1/1A drillhole. However, the first formed minerals from the Vestmanna-1 borehole are overgrown by abundant chabazite and thomsonite. Neglecting these later deposits, changes the zonation from a simple chabazite-thomsonite zone to an alternation between the mesolite and stilbite-heulandite zones.

The distribution of minerals, zones and temperatures

Frequency of occurrence of minerals

Table 2 shows the 17 zeolites and 8 associated minerals that were recorded in amygdales and mineralised fractures of the basalt in the islands of Suðuroy, Sandoy, Vágar, Streymoy, Eysturoy, Borðoy and Viðoy. In addition to the minerals listed, prehnite, pumpellyite, native copper and pyrite were found in the Lopra-1/1A borehole. All the zeolites listed in Table 2 have been reported previously from the Faroe Islands with the exception of garronite,

wells mapped. The most probable temperature range of deposition of the zeolite zones is indicated in Fig. 2.

The rules of zone classification stated above could not be followed strictly everywhere. In the southern part of Suðuroy, mineralised vesicles are rare and, in this area, the mapping had to be based mainly on mineralised fractures. In the Lopra-1/1A borehole, the study was based on cuttings. They included fragments of amygdales and mineralised fractures, and the first formed index mineral could
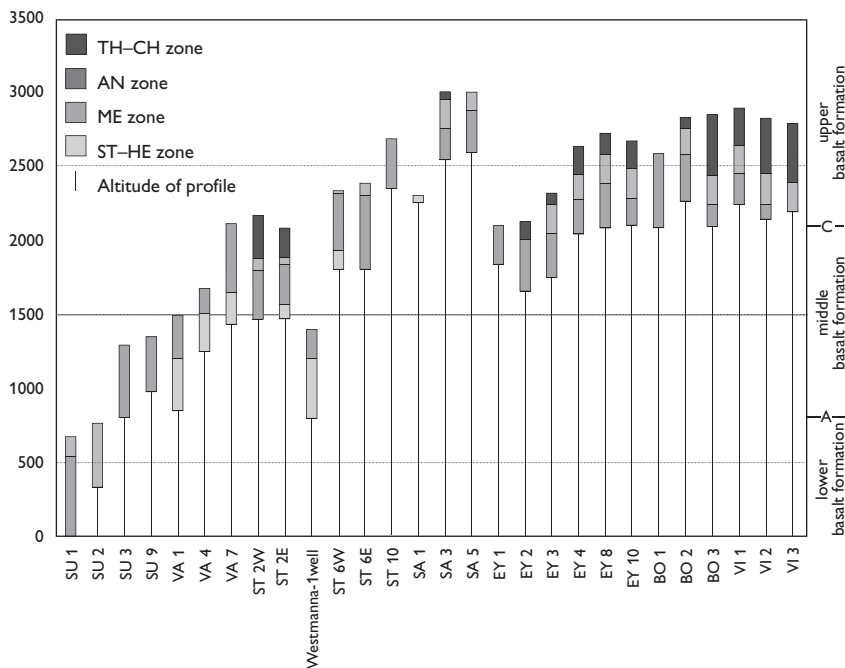
Fig. 4. Stratigraphic location of the zeolite zones in the 28 sections through the exposed part of the Faroe Islands. The data shown here are tabulated in Table 3.

which was found for the first time at several localities during the mapping reported here.

The minerals in Table 2 were divided into three classes: (1) very frequent minerals that occur at 60% or more of the localities; (2) common minerals that occur at between 15% and 60% of the localities; (3) rare minerals that occur at less than 15% of the localities. The frequency of occurrence is given as percentages of localities examined on each island.

From the column named *average* in Table 2, it is seen that chabazite, mesolite and thomsonite are the most frequent secondary minerals within the exposed part of the Faroe Islands, followed by stilbite, stellerite, heulandite, analcite and calcite. Epistilbite and scolecite are rare minerals in the exposed part of the Faroe Islands, but they are common in the Lopra-1/1A well.

Regional distribution of minerals and zones

Fig. 3 shows how the relative frequency of a number of index minerals and associated minerals varies from island to island. For most of the minerals, the relative frequency decreases from south to north and from west to east, but for the minerals of the analcite and the chabazite-thomsonite zone, the relative frequency increases in the direction of Viðoy (Fig. 1). The variation in relative frequency of minerals reflects the regional shift in the distribution of mineral zones. The analcite and mesolite zones are the

dominant mineral zones on Suðuroy. From Sandoy to Vágar, the analcite zone is gradually replaced by a stilbite-heulandite zone that becomes widespread on Vágar. On Streymoy and Eysturoy the stilbite-heulandite zone has a less widespread distribution, so that the stilbite-heulandite and the mesolite zones are of equal importance. The areal extent of the mesolite and stilbite-heulandite zones is further reduced on Borðoy and Viðoy, so the chabazite-thomsonite zone becomes the major one on these two islands.

Description of mineral assemblages and zones

Figures 5–11 show the geographic distribution of the mineral zones on the islands Suðuroy, Sandoy, Vágar, Streymoy, Borðoy and Viðoy. In order to show the vertical distribution of the mineral zones, 28 local sections were constructed that are also shown on Figs 5–11. The sections have been arranged such that it is possible to follow the changes in the mineral zones both geographically and stratigraphically (Fig. 4). The data on which the sections are based are shown in Appendices A and B, and Table 3 gives the thickness of each zone.

In contrast to the profiles drilled by the Lopra-1/1A and Vestmanna-1 boreholes, the profiles from the exposed part of the Faroes have been constructed from observations along each section line, so the sections do not represent a single vertical profile through the lava pile.

Table 3. Stratigraphic position and thickness of mineral zones (see Fig. 4)

Section	Base level Stratigraphic height in m[*]	ST-HE zone Thickness in metres	ME zone[†] Thickness in metres	AN zone Thickness in metres	CH–TH zone Thickness in metres
SU1+LO	0	–	530[†]	180	–
SU2	330	–	–	430	–
SU5	798	–	480	–	–
SU9	970	–	373	–	–
VÁ1	842	350	300	–	–
VÁ4	1241	250	180	–	–
VÁ7	1424	219	463	–	–
ST2W	1461	–	325	82	293
ST2E	1461	100	272	50	200
Vestmanna-1	795	400	200	–	–
ST6W	1799	125	385	20	–
ST6E	1799	–	500	83	–
ST10	2344	–	340	–	–
SA1	2252	50	–	–	–
SA3	2545	–	200	200	46
SA5	2594	–	280	116	–
EY1	1831	166	270	–	–
EY2	1650	50	350	125	–
EY3	1745	–	300	195	75
EY4	2039	–	230	170	193
EY8	2080	–	300	190	149
EY10	2098	–	180	200	187
BO1	2084	–	503	–	–
BO2	2263	–	310	182	70
BO3	2091	–	150	190	415
VI1	2237	–	100	190	251
VI2	2140	–	–	208	375
VI3	2188	–	–	200	400

[*] Stratigraphic height within the exposed lava pile of the Faroe Islands.
[†] The mesolite zone is composed of the upper 330 m of the Lopra-1 mesolite zone plus the 200 m thick mesolite zone of section SU1.

Suðuroy (Fig. 5)

The distribution of the secondary minerals on Suðuroy is remarkably heterogeneous, a feature noted by Currie (1905). To the north of section SU2 that extends across the island from Fámjin to Holmssund, nearly all vesicles and fractures of the basalts are mineralised, but to the south of the section, amygdales and mineralised fractures are rare.

The boundary (section SU2) between the two parts of Suðuroy forms a transition zone in which the scattered vesicles are partly mineralised by an analcite assemblage composed of hair-like mesolite, thomsonite, analcite, chabazite, calcite, quartz and chalcedony. This mineral assemblage is found all along section SU2, which means that no relationship exists between the secondary minerals and their stratigraphic position within the lava pile.

To the north of section SU2, the number of mineral species and the degree of mineralisation increases gradu-ally northwards and the area just north of Trongisvágs-fjørður is in the mesolite zone. Despite apparent regularity, the northern part of Suðuroy is a mosaic of small areas in which the mineral assemblages vary from place to place. The largest area of this kind occurs around the summit of Gluggarnir (443 m). At this locality, nearly all minerals listed in Table 2 are present.

The southern part of the island is partly devoid of zeolites. The most abundant minerals are quartz, calcite and chalcedony, while mesolite, thomsonite, chabazite, analcite, heulandite and stilbite are less frequent. The mode of mineralisation is also different on the two parts of the island. On the northern part of Suðuroy, mineralised fractures and vesicles occur in equal numbers, whereas mineralised fractures are more common than amygdales on the southern part of the island, in spite of the fact that empty vesicles occur at many localities. Because of this, section SU1 is based mainly on mineralised fractures.

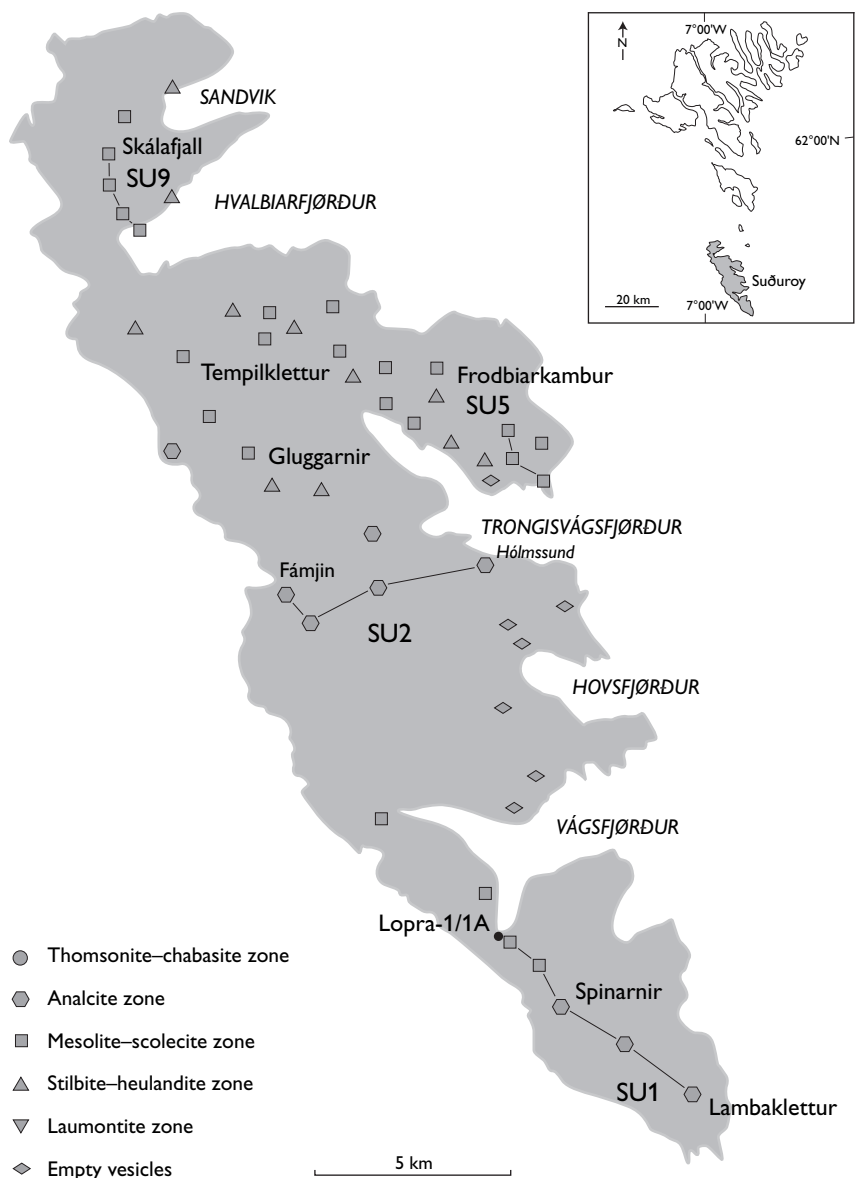Despite the weak amount of mineralisation on south-

Fig. 5. Distribution of zeolite zones on Suðuroy and on sections SU1, SU2, SU5, SU9 and in the Lopra-1/1A borehole.
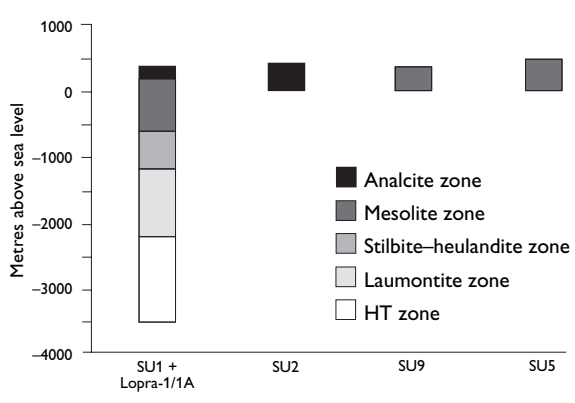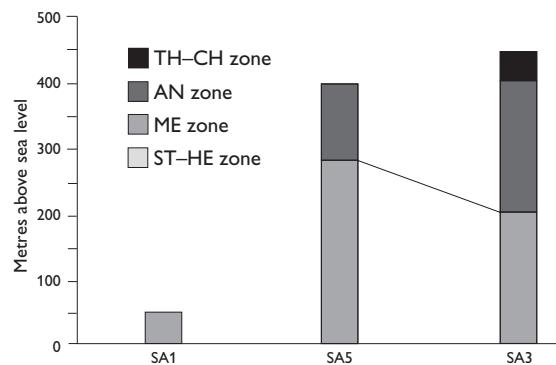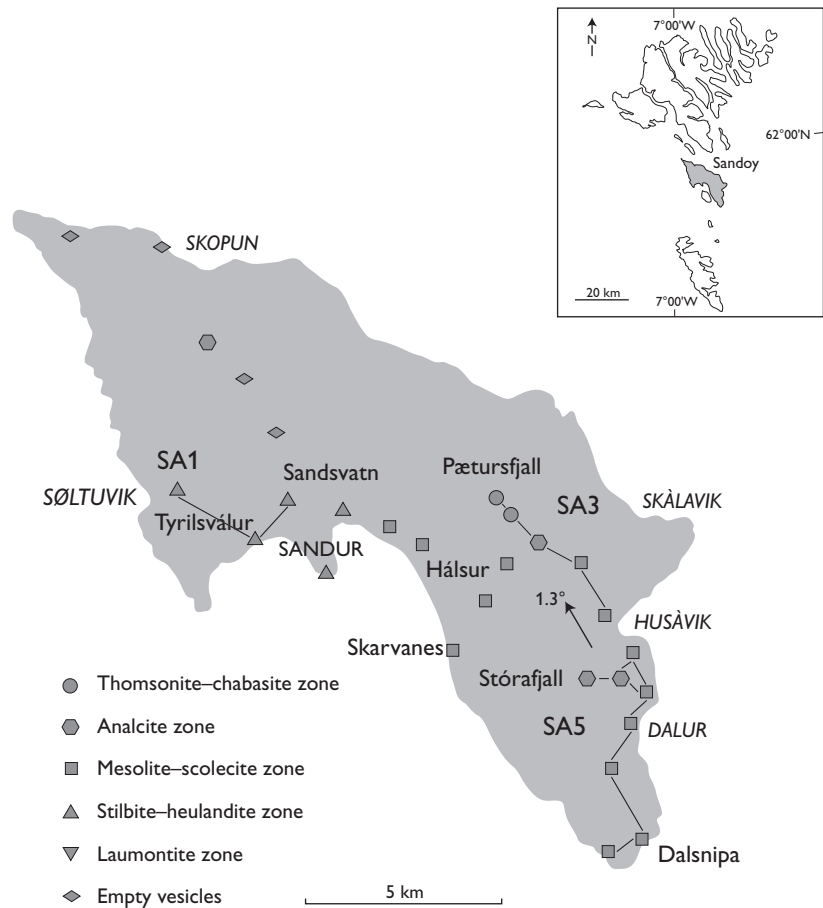
Fig. 6. Distribution of zeolite zones on Sandoy and on sections SA1, SA3 and SA5. The arrow indicates the apparent dip of the zeolite zones on section SA3.

ern Suðuroy, a clear zonation can nevertheless be discerned along section SU1, where a 200 m mesolite zone is overlain by a 180 m analcite zone. The mesolite zone continues to a depth of 600 m below sea level in the Lopra-1/1A borehole (Fig. 5). The most abundant minerals there are mesolite, scolecite, stilbite, heulandite and mordenite. Chlorite, mesolite and scolecite were deposited first. Mesolite and scolecite are replaced by laumontite as the first formed mineral at a depth of –626 m, indicating the top of the stilbite-heulandite zone. At about –1200 m, epis-

tilbite replaces stilbite as the first formed mineral so that the order of deposition becomes celadonite/chlorite-epistilbite-thomsonite-laumontite or celadonite/chlorite-epistilbite-laumontite-stilbite. Since an epistilbite zone has not yet been defined elsewhere, it was decided to include the total interval between –1200 m and –2200 m depth in the laumontite zone. A high temperature assemblage of laumonite, mordenite-prehnite, pumpellyite, chlorite, calcite and quartz is found from about –2200 m to the bottom of the Lopra-1A borehole at –3534 m.
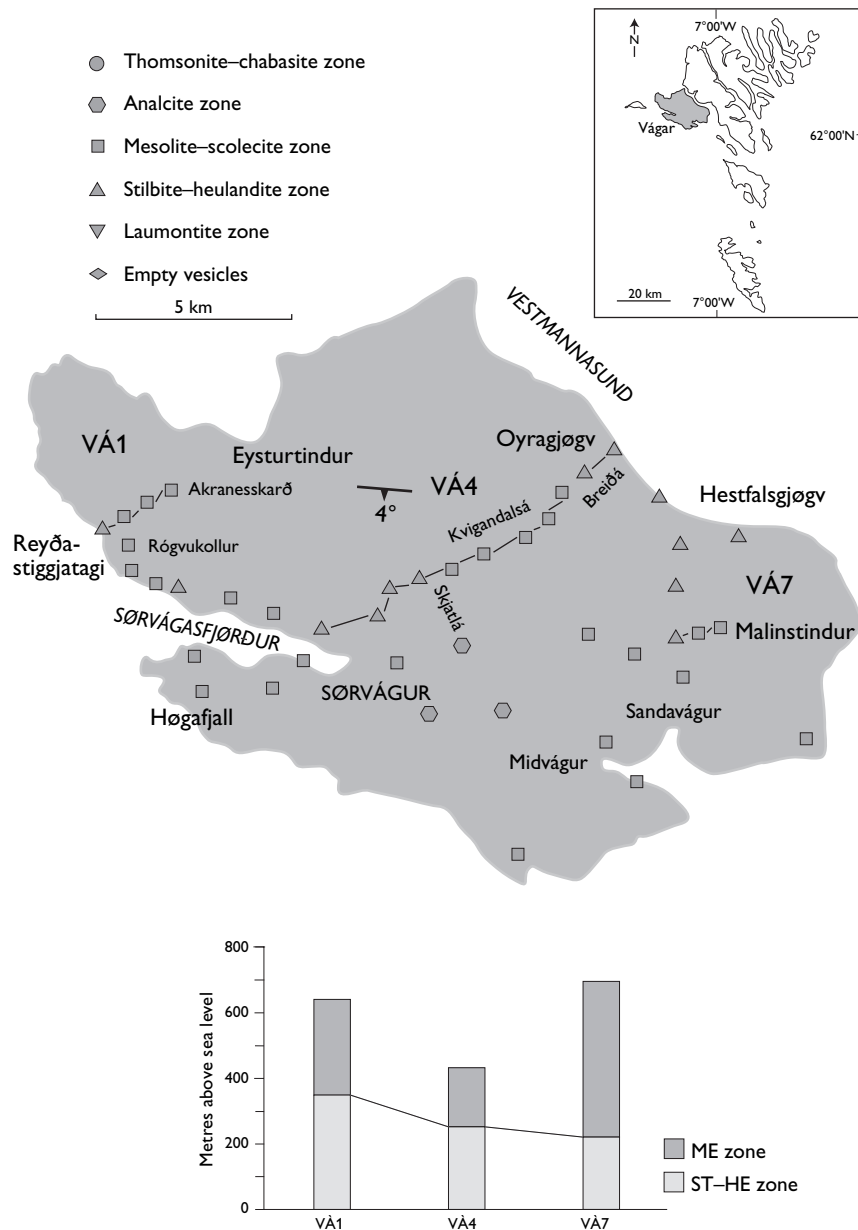
Fig. 7. Distribution of zeolite zones on Vágar and on sections VÁ1, VÁ4 and VÁ7. The dip and strike of the zeolite zones is indicated on the map.

The uppermost mineral zone preserved in the SU1 section is part of an analcite zone. In East Iceland, a chabazite-thomsonite zone (Walker 1960) and in East Greenland a zeolite free zone (Neuhoff *et al.* 1997) has been recorded in the uppermost parts of the basalt complexes whose total thicknesses are 700 m and 1400 m, respectively. If equivalent zones have ever existed on the southern part of Suðuroy, they must have been considerably thinner than those on Iceland and Greenland, because the palaeosurface of the lower basalt formation was about 300 m above the A-horizon (see below).

Sandoy (Fig. 6)

The southern part of Sandoy is strongly mineralised while the mineralisation in the northern part is weak. The area north of a line from Søltuvík to Skálavík is weakly mineralised by quartz, calcite, chalcedony, chabazite, hair-like mesolite, thomsonite and late formed stilbite or stellerite. Nearly all fractures and vesicles are totally mineralised to the south of the line. The most abundant zeolites are analcite, chabazite, heulandite, mesolite, stilbite and thomsonite. No distinct boundary has been observed between the northern and the southern part of the island.

Sections SA1, SA3 and SA5 (Fig. 6) show that four

zeolite zones exist on Sandoy. In the area between Sandur and Søltuvik, the uppermost 50 m of a stilbite-heulandite zone are exposed. The stilbite-heulandite assemblage consists of chlorite, heulandite, stilbite, mordenite and occasionally of laumontite and apophyllite. The latter two minerals occur mostly in fractures in the basalt.

However, the degree of mineralisation is low in the stilbite-heulandite zone and, by volume, only half of the vesicles are mineralised.

The southern and the eastern parts of Sandoy are dominated by a mesolite zone. The most abundant minerals are chabazite, heulandite, mesolite (solid or hair-like), stellerite, thomsonite and calcite together with minor gyrolite, gismondine and levyne. Heulandite and mesolite are the first deposited minerals. Dalsnípa at the south-east coast of Sandoy is the type locality of levyne (Brewster 1825). A detailed quantitative analysis of the mineral assemblage and the zeolite zones in section SA3 is given below.

Vágar (Fig. 7)

In contrast to Suðuroy and Sandoy, Vágar is totally mineralised and the island may be divided into two areas. Northeast of a line from Sørvágur to Sandavágur, a stilbite-heulandite assemblage occurs at 40% of the localities that has not been observed farther south. South-east of the boundary line, the localities are dominated by a mesolite and analcite assemblage. Around Miðvágur hair-like mesolite with up to 100 mm long crystal needles can be found in larger fractures and cavities in the basalt.

The distribution pattern of the mineral assemblages on Vágar is controlled by the rise of the stilbite-heulandite zone towards the north-east. A calculation shows that the stilbite-heulandite zone dips from between 1–3°SSW to 0.6°ESE, while the basalt flows dip 3–4°ESE, i.e. the mineral zones are discordant to the lava stratification.

A quantitative analysis of the mineral assemblage and the zeolite zones on section VÁ1 is given below.

Streymoy (Fig. 8)

Streymoy can be divided into a northern, a central and a southern area. A stilbite-heulandite assemblage occurs along the coast from Tjørnuvík to Langasandur in the north. The observed minerals are stilbite, heulandite, thomsonite, compact mesolite, laumontite, gyrolite, okenite, tobermorite, apophyllite, celadonite and smectite. The mineral assemblage in the amygdales changes gradually towards the west. The hydrated calcium silicates, stilbite and laumontite, disappear from the amygdales although they still occur in fractures in the basalt. At Saksun near the north-west coast, the stilbite-heulandite assemblage is replaced by a mesolite assemblage, characterised by solid mesolite, thomsonite, heulandite, chabazite, calcite and montmorillionite. Gyrolite and stilbite are present, but only in fractures. The distribution pattern is reversed in the central part of Streymoy (between Langasandur, Vestmanna, Dalsnipa and Kollafjørður). There the stilbite-heulandite assemblage occurs along the west coast from Vestmanna to Dalsnipa, while a mesolite assemblage is found along the east coast between Langasandur and Kollafjørður.

Only the mesolite assemblage is found in the southern part of Streymoy. Because of the differences in mineral distribution, sections ST2 and ST6 have been divided into two columns, showing the eastern and the western parts of the sections, respectively (Fig. 8). The dip of the zeolite zones in the northern part of Streymoy is 2°SW and 2°NNE the central area.

The distribution of secondary minerals is rather complex at many localities in northern and central Streymoy and shows *repetitive zoning*, i.e. a regular repetition of two mineral zones. For example, on the path from Saksun to the summit of Borgin (643 m), a mesolite zone is first encountered, then a stilbite-heulandite zone, then, near the summit, a second mesolite zone. Repetitive zoning has also been observed at Loysingafjall (638 m), where the mesolite zone is overlain by a stilbite-heulandite zone, and along the main road between the villages of Vestmanna and Kvívík. Between Vestmanna and Kvívík, zones occur within which the vesicles and fractures of the basalt flows are mineralised, either by heulandite, stilbite, mordenite plus minor laumontite, or by compact mesolite, heulandite, stilbite, thomsonite and chabazite. The widths of the zones are from a few hundred metres to about 1 km.

Repetitive zoning also exists in the Vestmanna-1 borehole. The first classification of the Vestmanna-1 mineral assemblages was based on the mass concentration of major index minerals. Since chabazite and thomsonite are the most abundant minerals, the entire mineral assemblage was classified as a thomsonite-chabazite assemblage. During the reclassification based on the first formed minerals for the present work, it became apparent that the drilled lava succession contains a repetitive zoning of mesolite and stilbite-heulandite assemblages (Fig. 8).

It is unlikely that repetitive zoning is caused by vertical fluctuations of the geothermal gradient within such relatively short distances, but the repetitive zoning may reflect flows of water of different temperature that changed
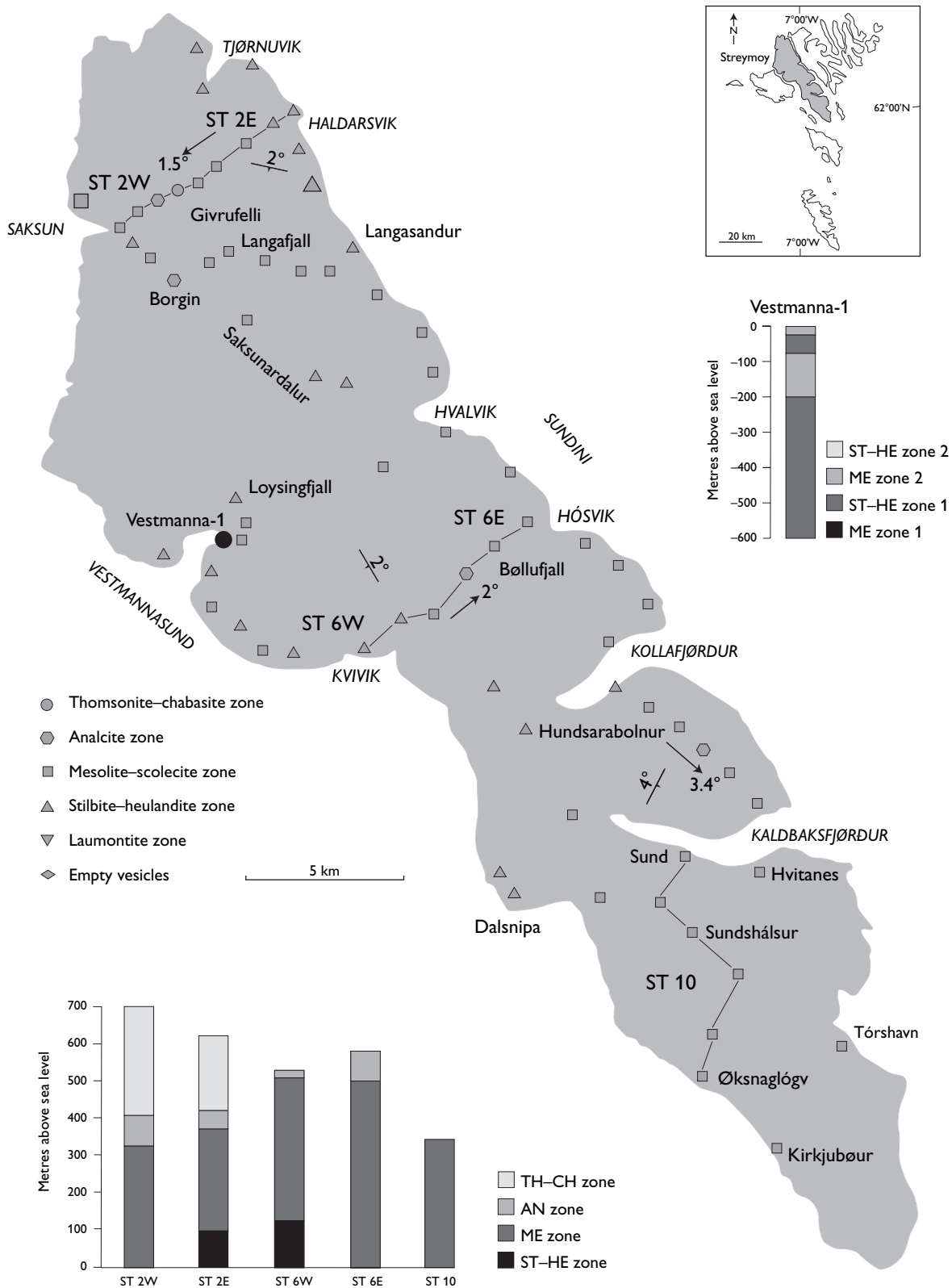
Fig. 8. Distribution of zeolite zones on Streymoy and on sections ST2E, ST2W, ST6E, ST6W, ST10 and in the Vestmanna-1 borehole. The dip and strike of the zeolite zones is indicated on the map. The arrows indicate the calculated strike of the zeolite zones between the sections.

Fig. 9. Distribution of zeolite zones on Eysturoy and on sections EY1, EY2, EY3, EY8 and EY10. The dip and strike of the zeolite zones is indicated on the map. The arrows indicate the calculated dip of the zeolite zones between the sections.
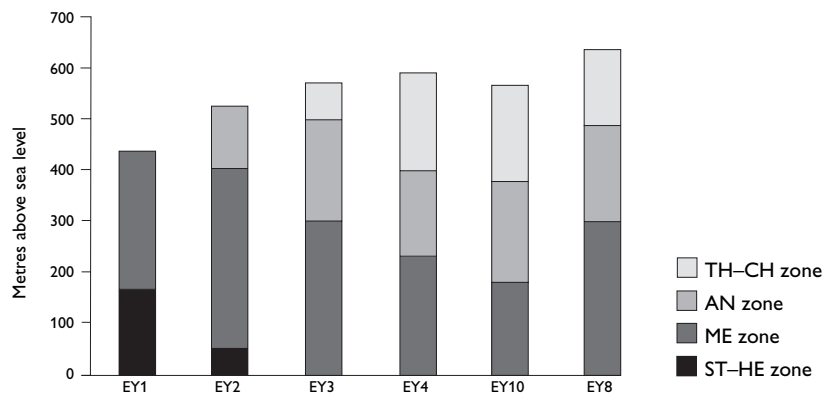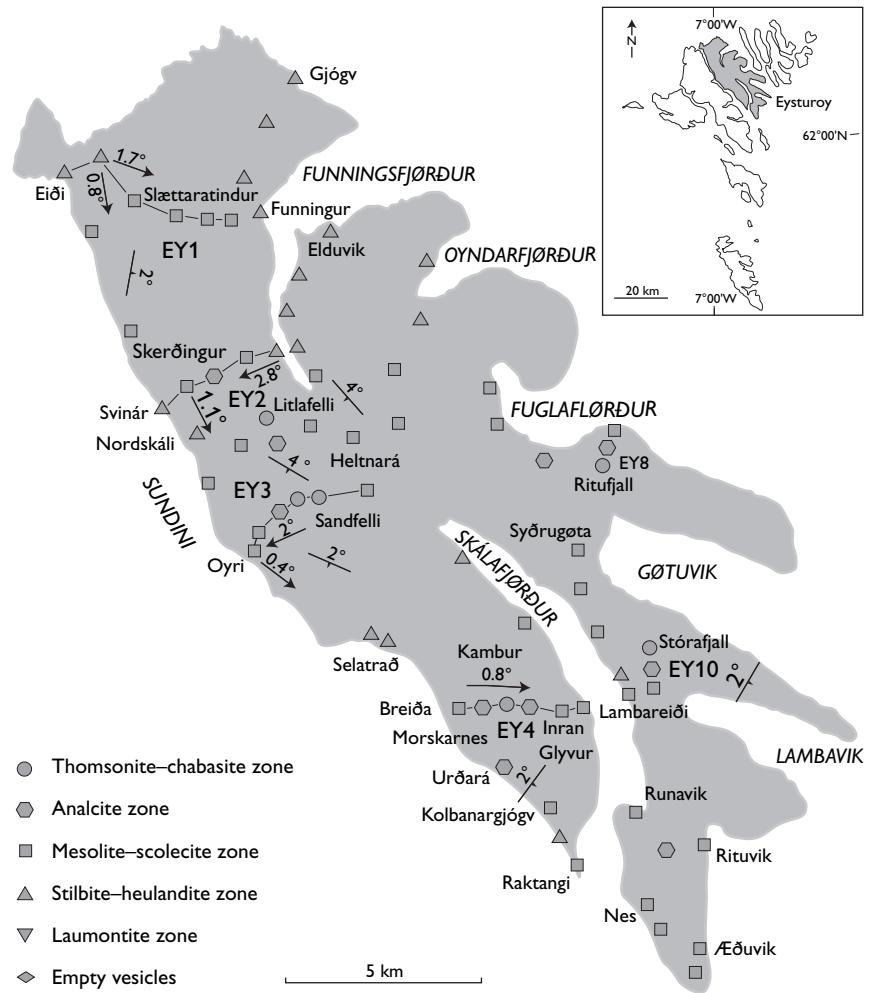
locally the vertical distribution of temperature. Alternative explanations for repetitive zoning are: (1) local variations in the chemical composition of the basalt, or: (2) mineralisation in an open and closed system, caused by variations in the percolation speed of the geothermal water (Barth-Wirsching & Höller 1989; Gottardi 1989).

Eysturoy (Fig. 9)

Eysturoy may be divided into two for descriptive purposes. North of a line from Norðskáli to Fuglafjørður, the stilbite-heulandite assemblage occurs at 64% of localities. South of that line mineral assemblage occurs at only 12% of the localities (Fig. 9). The actual strike and dip of the
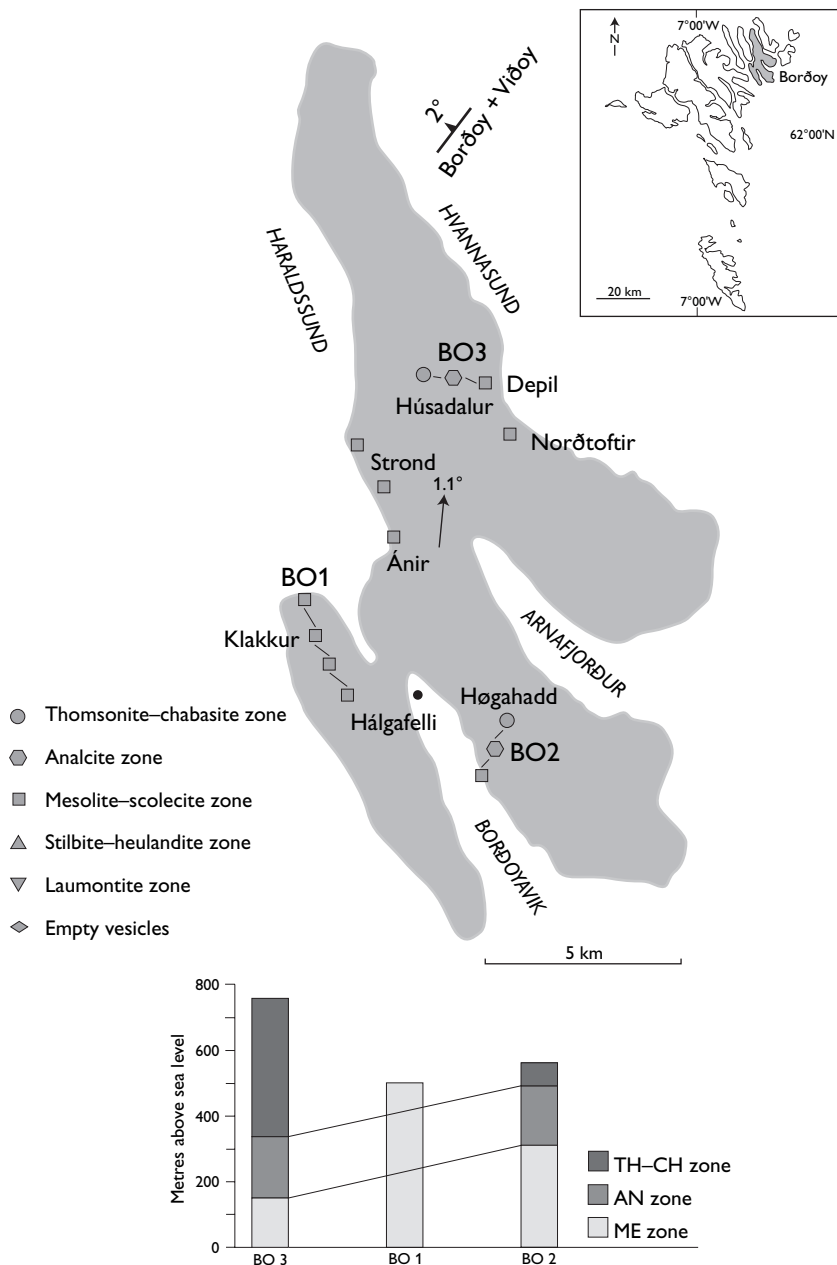
Fig. 10. Distribution of zeolite zones on Borðoy and on sections BO1, BO2 and BO3. The arrow shows the strike of the zeolite zones between BO2 and BO3. The common dip and strike of the zeolite zones on Borðoy and Viðoy is shown in the upper right corner.

zeolite zones can be determined by combining the dip of the zeolite zones along the sections with the dips between them. On Fig. 9 it can be seen that the strikes and dips change to follow the changes in mineralogy. North of a line from Svinár/Norðskáli to Fuglafjørður, the zeolite zones dip about 2° towards the east. To the south of the line, the dips of the zones shift gradually from 4° to the SW to 2° to the S. This means that the mineral zones are discordant to the lava bedding on the northern part of Eysturoy, but nearly concordant to it on the southern part of the island.

Borðoy (Fig. 10)

The mesolite, analcite and chabazite-thomsonite zones are the only ones exposed on Borðoy. At Klakkur (section BO1) the vesicles and fractures in the basalt are mineralised by heulandite, stilbite, mesolite (massive and hairlike), thomsonite (massive and hair-like), chabazite, levyne, phillipsite, montmorillionite and celadonite, but no clear relationship exists between the distribution of mineral and height in the lava pile. Since analcite and mesolite are the first deposited minerals in most vesicles, the mineral assemblage of section BO1 was classified as a mesolite zone assemblage. The poor zoning west of Borðoyavik suggests

Table 4. Quantitative analysis of section SA3, Sandoy. The table shows the number of observed
and calculated amygdales containing the index mineral per 25 amygdales

Altitude metres	Me N_{obs}	N_{cal}	Me* N_{obs}	N_{cal}	Th N_{obs}	N_{cal}	Th* N_{obs}	N_{cal}	An N_{obs}	N_{cal}	Ch N_{obs}	N_{cal}
0	18	21.3	0	0.0	14	13.4	0	0.1	14	12.8	0	1.1
25	18	18.6	0	0.0	12	11.3	0	0.1	0	11.5	0	1.3
50	10	15.5	0	0.02	8	9.2	0	0.1	11	10.2	1	1.5
75	16	12.2	0	0.1	5	7.2	0	0.2	8	9.2	1	1.8
100	0	9.1	0	0.3	4	5.5	0	0.3	0	8.2	0	2.1
120	4	6.6	0	0.8	3	4.3	0	0.5	8	7.4	2	2.4
150	6	4.1	2	1.4	3	2.8	0	0.7	5	6.3	3	2.7
180	2	2.4	3	5.9	1	1.7	2	1.0	5	5.2	0	3.6
200	0	1.3	7	10.3	1	1.1	3	1.5	4	4.5	0	4.2
210	2	1.1	14	13.0	0	0.9	2	1.8	5	4.2	0	4.4
220	1	0.6	15	15.9	0	0.7	0	2.2	0	3.8	6	4.8
243	0	0.4	22	21.4	0	0.5	3	2.8	3	3.3	6	5.4
270	1	0.1	22	24.9	0	0.2	5	4.4	3	2.5	6	6.7
320	1	0.0	10	11.9	0	0.1	9	8.5	2	1.5	8	9.3
340	1	0.0	5	5.6	0	0.0	10	11.2	1	1.1	13	11.3
360	0	0.0	0	2.0	0	0.0	0	14.0	0	0.9	0	12.0
375	0	0.0	1	0.7	0	0.0	14	16.3	0	0.7	0	13.2
380	0	0.0	1	0.5	0	0.0	14	17.1	0	0.7	0	13.8
400	0	0.0	0	0.1	0	0.0	23	20.1	1	0.4	16	15.4
420	0	0.0	0	0.0	0	0.0	23	22.8	0	0.3	0	17.2
446	0	0.0	0	0.0	0	0.0	23	24.6	0	0.3	20	19.1
$R_{N,U}$†	–	0.988	–	0.996	–	0.875	–	0.991	–	0.982	–	0.952
S_H‡	–	44	–	17	–	14	–	32	–	56	–	59

† $R_{N,U}$: Correlation coefficient of the regression line lnH versus $U(N_{obs})$. See equation (2).
‡ S_H: Standard deviation on Hcal. in m. See equation (3).

Table 5. Quantiative analysis of section VÁ1, Vágar. The table shows the number of observed
and calculated amygdales containing the index mineral per 25 amygdales

Altitude metres	Ch N_{obs}	N_{cal}	Th N_{obs}	N_{cal}	Me N_{obs}	N_{cal}	He N_{obs}	N_{cal}	St N_{obs}	N_{cal}
10	0	0.2	0	0.8	0	0.0	4	3.7	3	3.7
100	0	0.3	0	1.7	0	0.1	9	11.3	15	14.3
200	0	0.6	0	3.9	0	0.3	24	22.7	21	25.0
235	0	0.7	3	3.9	0	0.4	23	24.8	0	23.2
340	0	1.2	13	10.1	0	1.9	15	17.7	7	6.7
350	0	1.2	9	10.7	1	2.2	18	16.3	5	5.4
380	2	1.4	15	12.6	3	3.1	10	11.9	0	2.6
410	2	1.7	0	14.8	6	4.5	7	7.9	0	1.1
460	3	2.2	19	18.4	7	7.6	3	3.1	0	0.2
475	3	2.4	18	19.4	9	8.8	2	2.2	0	0.1
500	6	2.7	19	21.1	10	11.0	1	1.2	0	0.0
550	3	3.5	21	23.8	0	16.1	0	0.2	0	0.0
610	5	4.8	0	25.0	24	22.0	0	0.0	0	0.0
630	6	5.3	23	24.8	0	23.5	0	0.0	0	0.0
$R_{N,U}$†	–	0.987	–	0.972	–	0.851	–	0.837	–	0.871
S_H‡	–	58	–	27	–	25	–	26	–	97

† R_N: Correlation coefficient of the regression line lnH versus $U(N_{obs})$. See equation (2).
‡ S_H: Standard deviation on Hcal. in m. See equation (3).

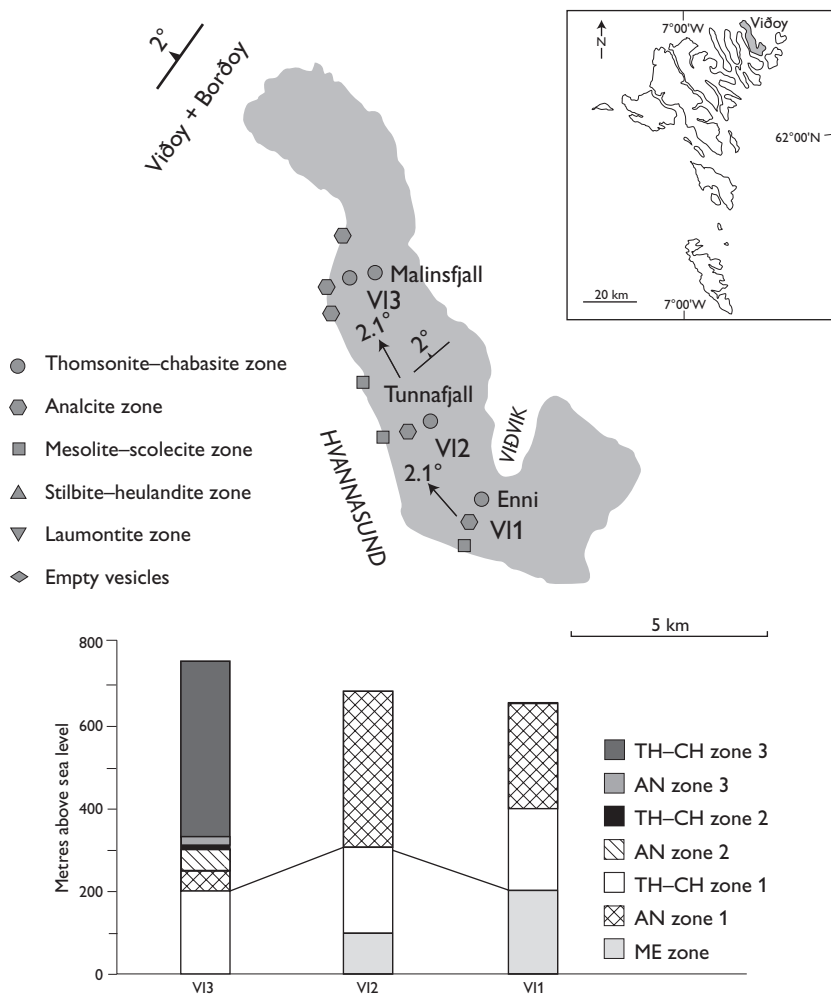Fig. 11. Distribution of zeolite zones on Viðoy and on sections VI1, VI2 and VI3. The dip and strike of the zeolite zones is indicated on the map. The arrows indicate the strike of the zeolite zones in the profiles. The common dip and strike of the zeolite zones on Borðoy and Viðoy is shown in the upper left corner.

that the area has been affected by several generations of mineralisation.

The zoning becomes distinct farther eastwards on sections BO2 and BO3. The exposed part of the mesolite zone is 500 m on BO1, but 300 m on BO2 and 150 m on BO3 (Fig.10). The analcite and thomsonite-chabazite zones also appear at higher levels on sections BO2 and BO3. The mineral zones have apparent dips of about 1º towards the north and east. The analcite zone is about the same thickness on both BO2 and BO3, which suggests that the vertical displacement of the two zones reflects differences in altitude of the palaeosurface of the basalt plateau. The lava flows of Borðoy dip 1.6º to the SE, which means that the zeolite zones are discordant to the lava bedding.

Viðoy (Fig.11)

The distribution pattern of the secondary minerals on Viðoy is a continuation of that on Borðoy. The mineral zones are displaced downwards compared to those of Borðoy with the result that only between 100 m and 200 m of the mesolite zone is exposed on sections VI1 and VI2. On section VI3 a lower analcite zone about 200 m thick is exposed, which is separated from the thomsonite-chabazite zone by about 130 m of repetitive zoning. The chabazite-thomsonite zone is about 430 m thick, which is the maximum thickness recorded for that zone within the basalts exposed on the Faroe Islands.

Quantitative analysis of mineral distributions

Once the position and temperatures are known of the boundaries of the zeolite zones, the geothermal gradient

138

and the altitude of the palaeosurface of the basalt plateau can be estimated using least squares regression, assuming a linear palaeotemperature gradient. However, in order to make a reliable estimate, the regression must be based on three or more zone boundaries. This requirement is fulfilled only where the Lopra-1/1A and SU1 sections can be combined. Elsewhere, the number of exposed zone boundaries is too small to calculate a geothermal gradient. In order to overcome this limitation, an attempt has been made to estimate the position of unexposed mineral boundaries from a detailed analysis of the distribution of the exposed mineral zones.

Quantitative analyses carried out on the mineral assemblages of the Lopra-1/1A and Vestmanna-1 boreholes showed that the relative vertical frequency of the minerals followed a skewed distribution with one or more maxima (Jørgensen 1984). This observation has been used to extrapolate non exposed zone boundaries on section VÁ1 on Vágar and SA3 on Sandoy. The two sections were chosen because they are through the middle and the upper basalt formations respectively, the distribution of minerals in them is simple and nearly all rocks sampled contain a large number of well developed amygdales. In order to examine the relationship between the thickness of the zeolite zones and the distribution of index minerals, the number of amygdales containing a particular index mineral was recorded for 25 amygdales (see below). To ensure that the amygdales were selected randomly, all amygdales in the samples from each locality were numbered and the 25 amygdales for examination were selected by using a computerised random number generator. After the amygdales had been chosen, the first formed index mineral was determined and the total number of amygdales containing the same index mineral was recorded. These results are presented as columns N_{obs} in Tables 4 and 5.

Trials were carried out using different exponential distribution functions to find the best correlation between altitude and number of amygdales containing the same index minerals. The experiments showed that the best fit between the observed distribution and the calculated distribution was obtained by the log normal distribution function:

$$N_{i,cal} = N_0 \exp(-\tfrac{1}{2}[(\ln H - \ln H_0) / a]^2) \qquad (1)$$

where:

$N_{i,cal}$ is the calculated number of amygdales containing index mineral i.

N_0 is the total number of amygdales investigated; in this case $N_0 = 25$.

H is the altitude of the sample above sea level.

H_0 is the altitude where the distribution function attains its maximum value.

a is a constant.

By transforming equation (1) to a linear form and replacing $N_{i,cal}$ by $N_{i,obs}$, we obtain:

$$\ln H = aU + \ln H_0, \text{ where } U = \pm [2 (\ln N_0 - \ln N_{i,obs})]^{\frac{1}{2}} \quad (2)$$

The constants a and H_0 can be determined by linear regression on U and lnH. The calculated number of amygdales ($N_{i,cal}$) containing index mineral i is shown in Tables 4 and 5. A t-test shows that U and lnH fit a straight line at the 1% confidence level.

The distribution curves in Figs 12 and 13 give only a best estimate for the height above sea level of the zone boundaries. To assess the degree of uncertainty of these estimates (see below) we calculate the standard deviation of the altitude (H) defined as:

$$S_H = [1/(n - 2) \, S \, (H - H_c)^2]^{\frac{1}{2}} \qquad (3)$$

where:

n is number of pairs (H, N_i) along the distribution curve.

H is the altitude of the sample above sea level.

H_c is the calculated altitude of a point on the distribution curves corresponding to N_i amygdales that contain index mineral i.

In equation (3), n is reduced by 2 because of the loss of two degrees of freedom by the least squares estimation of a and H_0 in equation (1) (Miller & Freund 1977).

When N_i, H_0 and a are known, H_c can be calculated from equation (1). S_H for the distribution curves is shown in Tables 4 and 5 and a graphic representation of the calculated distributions of chabazite, thomsonite, mesolite, analcite, heulandite and stilbite on sections SA3 and VÁ1 is shown in Figs 12 and 13. The shape of the curves suggests that a temperature range existed around the altitude H_0 in which conditions were favourable for the formation of a particular zeolite. Where $H < H_0$, palaeotemperatures decreased away from H_0 to where they became too low for the zeolite to form. Where $H > H_0$, palaeotemperatures increased away from H_0. The zeolite that was most stable at H_0 would have been formed in some interval below H_0 but, at higher temperatures, formation of the first zeolite would gradually be inhibited and another one would have become stable. So a zeolite will most likely be found between the maximum slopes of its distribution curve versus height, which corresponds to a palaeotemperature interval.
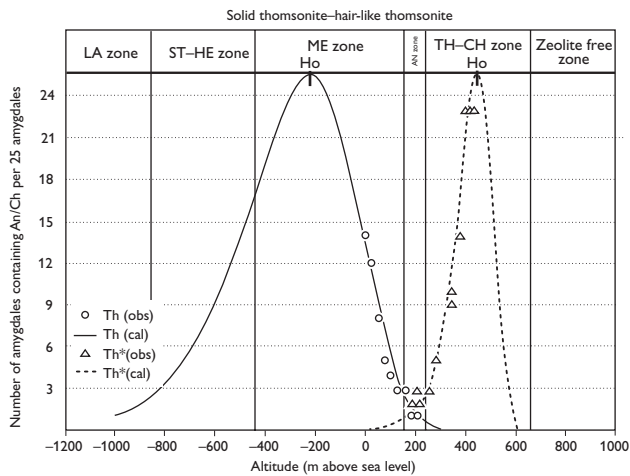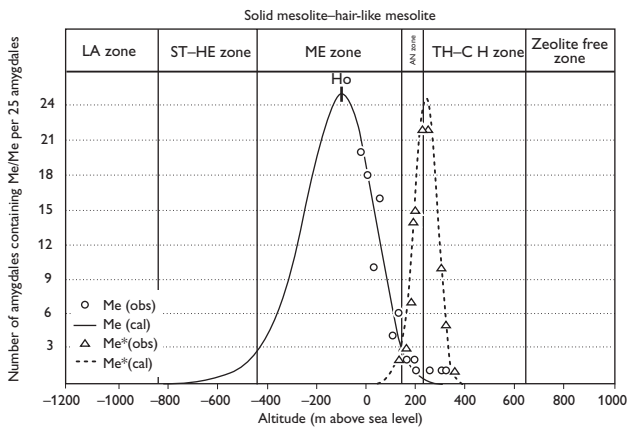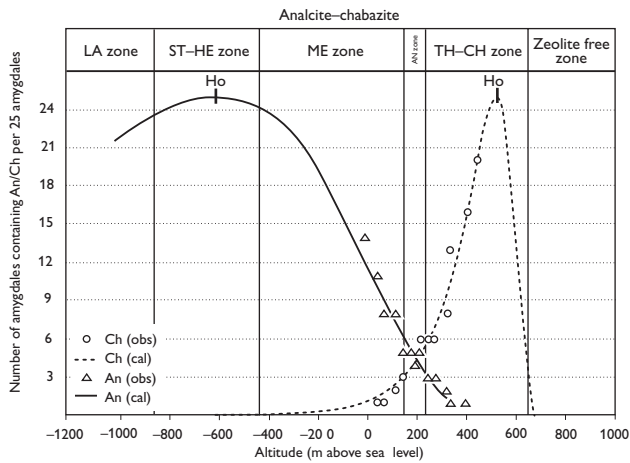
Fig. 12. The calculated distribution of chabazite, analcite, thomsonite (compact and hair-like) and mesolite (compact and hair-like) on section SA3, Sandoy.

The calculated distribution curves shown in Figs 12 and 13 show that the number of amygdales containing a particular zeolite decreases rapidly as $|H - H_0|$ increases. This has the practical consequence that it becomes harder to define a zone boundary by field mapping when sample
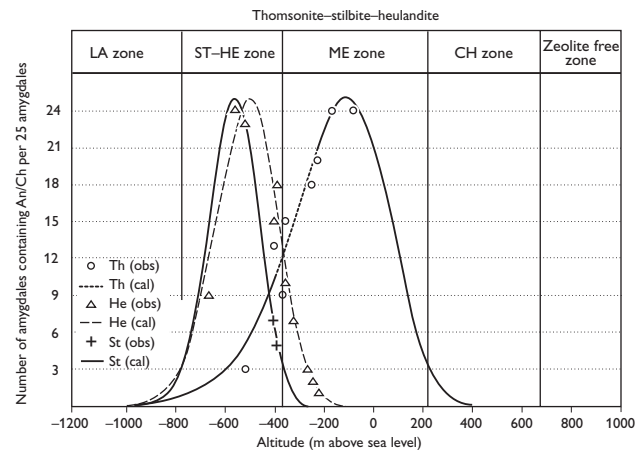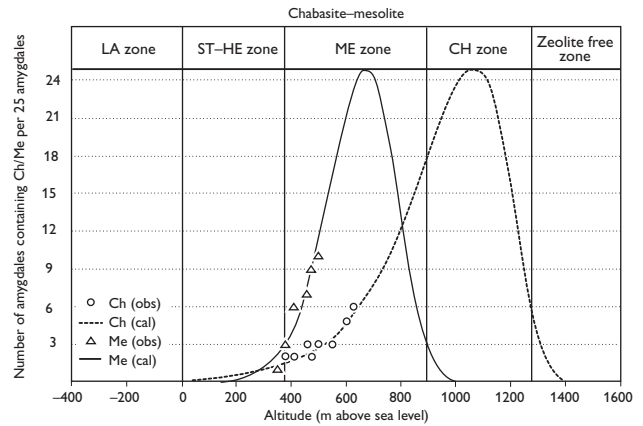
Fig. 13. The calculated distribution of chabazite, mesolite, thomsonite, stilbite and heulandite on section VÁ1, Váger.

numbers are small. A zone boundary is defined for mapping purposes to be reproducible with a probability of 95%. The probability (P) of discovering $N_{i,obs}$ objects (amygdales containing the new zeolite i) among N_0 objects (amygdales) can be calculated by means of the binomial distribution function (see e.g. Kreyszig 1975 or Miller & Freund 1977). It can be shown that when $N_0 = 25$ and $P = 95\%$, then $N_{i,obs} = 3$. Fig. 12 shows that this reasoning can be applied to define the upper boundaries of the thomsonite-chabazite, analcite and mesolite zones at the heights where the upper end of the appropriate distribution curve intersects the line $N_i = 3$. However, this method cannot be used on the upper boundaries of the stilbite-heulandite and laumontite zones, because stilbite, heulandite and laumontite do not exist as first formed index minerals in section SA3. Fig. 12 shows that solid mesolite occurs most commonly in the mesolite zone and thomsonite occurs most commonly in the stilbite-heulandite plus the mesolite zone. If we assume that 95% of the two index minerals occurs within the zones in question, we can define the

Table 6. Estimated palaeothermal gradients and the altitude of the palaeosurfaces at Lopra-1/1A and sections SU1, VÁ1 and SA3

Zeolite zone	Zeolite free	Ch–Th	Me	St–He	La	Palaeothermal gradient	Altitude of palaeosurface	Correlation coefficient
Temperatures at the zone boundaries	40–60°C	50–70°C	90–100°C	110–130°C	190–220°C	°C/km	m above sea level	R
Altitude of zone boundaries (m above sea level):								
Lopra-1/1A + SU1	–	–	–590	–1200	–2200	66 ± 9	443–983	0.9547
VÁ1	1325	900	380	–	–	63 ± 8	1760–2080	0.9181
SA3	653	150	–425	–825	–	56 ± 7	1150–1524	0.8689

heights of the lower boundaries of the mesolite and the stilbite-heulandite zones where the lower end of the distribution curves interest the line N_i = 3. That 95% of an index mineral occurs within the interval in question can be verified by plotting the accumulated distribution of the index mineral in a probability diagram.

Analcite occurs only sporadically below 340 m on section VÁ1 (Fig. 13), so the analcite zone cannot be defined on this profile. The other zone boundaries were calculated as described above.

Estimation of palaeothermal gradients and altitudes of palaeosurfaces

If we assume that the palaeothermal gradient was constant with depth, it may be estimated by linear regression on the data from the combined Lopra-1/1A plus SU1 sections, the mineral zone boundaries obtained by calculation and shown in Figs 12 and 13 and the temperatures shown in Fig. 2. The resulting estimates are shown in Table 6. The new estimate from southern Suðuroy is considered more accurate than that in Jørgensen (1984), which was based on the mineral distribution in the Lopra-1 borehole only. From these palaeogeothermal gradients and assuming a surface temperature of 7°C, the altitudes of the palaeosurface of the basalts has been estimated (Table 6).

The altitude differences between the estimated palaeosurface and stratigraphic marker horizons A and C is different at the three localities (Table 7). On southern Suðuroy, the palaeosurface was about 0.7 km (± 0.3 km) above present day sea level, i.e. close to the extrapolated top of the lower basalt formation. On Vágar, the palaeosurface was 1.9 ± 0.2 km above the extrapolated top of the lower basalt formation (or 0.5 ± 0.2 km above the top of the middle formation), while on Sandoy, the palaeosurface was 1.7 ± 0.2 km above the top of the middle basalt formation. This suggests that the focus of volcanism shifted laterally with time as will be discussed below.

Table 7. Estimated thicknesses of the basalt formations along various sections across the Faroe Islands

Area	Section	Formation	Altitude of palaeo surface in m above sea level (Table 6)	Present stratigraphic thickness in m	Local altitude (m) of A- and C-horizons	Altitude of palaeosurface in m above A- or C-horizon
S. Suðuroy	Lopra-1/1A + SU1	L. Formation	443–983	> 3100[1]	A-horizon: 700	A-horizon: –257–283
W. Vágar	VÁ1	M. Formation	1760–2080	1410[2]	A-horizon: 60	A-horizon: 1700–2020
E. Sandoy	SA3	U. Formation	1150–1525	700–900[1,3]	C-horizon: –400	C-horizon: 1550–1924

Sources: [1] Larsen *et al.* 1999, [2] Waagstein & Hald 1984, [3] Waagstein 1988.

Discussion

Palaeothermometry and zone boundaries

The use of zeolites as palaeotemperature indicators is based on the assumptions: (1) that the zeolite zones reflect univariant equilibrium with a high coefficient dP/dT of the Clausius-Clapeyron equation and and: (2) that the formation temperature of the minerals is independent of the chemical composition of the hydrothermal solution.

Assumption (1) is fulfilled because the properties of condensed systems are nearly independent of pressure, if the pressure is not extremely high and the temperature is below the supercritical temperature (374°C) of water. We can also estimate the error of the temperature determination when we ignore the external pressure of the system. The coefficient dP/dT is known only for a small number of systems that involve zeolites, but experimental studies of the systems stilbite-laumontite-H_2O and laumontite-wairakite-H_2O show that dP/dT is of the order of 25–33 bars/degree in the range P_{fluid} = 0–2000 bars (Liou 1971; Jové & Hacker 1997). Consequently, if the external pressure is equal to the fluid pressure and the original thickness of the lava pile is 2 km, the likely maximum error of the temperature determination is 8°C, disregarding the depth between the boundary of the zeolite zone and the unknown altitude of the palaeosurface.

In contrast to the effect of pressure, the chemical composition of the rock and the hydrothermal fluids has a much larger effect on the formation temperature of the minerals. Barth-Wirsching & Höller (1989) studied the formation of zeolites in glasses of different chemical compositions. They found that replacing rhyolitic glass by basaltic glass caused the formation temperature of different zeolites to increase by between 50°C and 100°C. This demonstrates the importance of choosing a reference area for the thermometry that consists of rocks with a chemical composition similar to that of the rocks in the area studied.

Other factors may also affect the formation of zeolites such as the texture of the rock, the content of glass and the porosity of the rock (Gottardi 1989).

The geothermal areas on Iceland were used as a reference for the thermometry in the present study. The basalts from the Faroe Islands are all tholeiites, but show large compositional variations that range from picritic to ferrobasaltic (Waagstein 1988). Most of the Icelandic basalts are also tholeiites, but minor amounts of acid rocks (rhyolites, andesites, granophyres, acid tuff) are found, mainly associated with volcanic centres (Sigurdsson 1967). This compositional variation of the Icelandic rocks may partly explain the large variation in temperature at the boundaries of the zeolite zones mentioned above (Fig. 2).

From the description of the sections shown in Figs 12 and 13 (and listed in Appendix A), it can be seen that the distribution of index minerals varies gradually between successive zeolite zones. An index mineral that defines a zone may thus overlap the boundaries of neighbouring zones which makes it difficult to define the exact boundaries between mineral zones. The problem was solved by statistical analysis on sections SA3 and VÁ1 from which the boundaries of the zeolite zones could be defined as the locations where 3 out of 25 amygdales contain the appropriate index mineral.

The overlap problem occurs in all the sections described in Appendix A and, because of the lack of quantitative mineral data, the distributions in SA3 and VÁ1 were the only ones that could be described by a simple distribution model. On all other sections, the zone division was based on a crude estimate of the abundance of the index minerals around the zone boundaries. Figs 12 and 13 show that the overlap between the zeolite zones varies from 100 m to 300 m. which means that, in the worst case, the zone boundaries could be determined with an accuracy of only ± 150 m when the zone boundary localities are based on a subjective estimate of the abundance of index minerals.

Volcanic and tectonic evolution

The average of the three calculated palaeogeothermal gradients is about 60°C/km and there may be a small decrease in the gradient from the lower to the upper basalt formation. If real, this decrease could reflect either a reduction in heat flow with time or a variation in heat flow with locality.

Rasmussen & Noe-Nygaard's (1969, 1970) summary of the volcanic evolution of the Faroe Islands that volcanic activity started in the west and moved eastwards with the times, must be modified, because evidence from the Lopra-1 drillhole indicates that the lavas of the lower formation were erupted from local centres (Waagstein 1988) and not from centres situated west of the present islands. This change might explain the change in the palaeogeothermal gradients shown in Table 6. The eruption centres of the lower and middle formations were located in the Faroe Islands and the geothermal gradient was high. Movement away to the east during eruption of the upper formation led to a decrease in the gradient.

Regional distribution of the zeolite zones

At the time when the Faroe lava pile was first mineralised, the thermal gradient seems to have been fairly constant, at least regionally and for some time. This is suggested by the rough equality of the calculated palaeogeothermal gradients from the southern, western and central part of the Faroes that represent different stratigraphic levels (Table 6). The overall regional distribution of zeolites is thus considered to reflect primarily variations in the maximum depth of burial of the basalt rather than differences in heat flow. The inferred palaeosurface on southern Suðuroy is close to the extrapolated top of the lower formation (Table 7), indicating that the total thickness of middle and upper formation lavas must have been small in this area. In contrast, in eastern Sandoy about 50 km farther north where the exposed thickness of the upper formation is of the order of 1 km, the estimated palaeosurface is >1.5 km above the base of the upper formation or stratigraphically approximately 3 km above the lower–middle formation boundary. If we use the palaeogeothermal gradient calculated on Sandoy, then the palaeosurface of the upper formation on Viðoy may have been at about 1.3 km ± 0.2 km above sea level. These results suggest that the upper formation had a similar or only slightly smaller thickness in the north-eastern part of the Faroes compared with the central part of the islands. On the other hand, the upper formation seems to have been much thinner or non existent in both the western and southern parts of the Faroes (Table 7) and the middle formation must also have been thin in the south.

The inferred thinning of the middle and upper formations from the central to southern part of the Faroes is consistent with a northerly source area for these basalts, centred on the rift between the Faroes and Greenland (Waagstein 1988; Hald & Waagstein 1991; Larsen *et al.* 1999). The thinning of the upper formation towards the west is consistent with Rasmussen & Noe-Nygaard's (1969, 1970) interpretation of an easterly source for this part of lava pile and may suggest a shift in the focus of volcanism.

The first order regional zeolite distribution pattern is affected by local perturbations of the mineral zone boundaries (Fig. 4). These perturbations show up as shifts in the dip of the zone boundaries within and between neighbouring islands as well as shifts in the degree of mineralisation. The latter effect is clearly seen towards the south. Southern Sandoy and northern Suðuroy are heavily mineralised, although at different temperatures, whereas the vesicles of the basalt in the adjoining areas of northern Sandoy and southern Suðuroy usually contain no zeolites.

On the northern and western islands, the zone distribution shows a tendency to symmetry around the narrow NW–SE-trending sounds that separate the islands (Figs 7–9). The distributions on the neighbouring north-eastern islands of Borðoy and Viðoy similarly seem to be mirror imaged, a distribution difficult to explain by variations in depth of burial. It is more likely that the distributions reflect local differences in palaeotemperature, perhaps related to the circulation of water underground with high temperatures in areas of up welling and low temperatures in areas of down welling. The symmetry of the zonal distribution patterns suggests that these temperature anomalies are in part related to NW–SE-trending eruption fissures or zones of weakness separating the present islands (Noe-Nygaard 1968; Rasmussen & Noe-Nygaard 1969, 1970). They are subparallel to the transfer zones in the Faroe–Shetland Basin described by Rumph *et al.* (1993) and later authors, and may indicate the presence of similar deep seated features. Both the regional and the local distribution of zeolite assemblages probably reflect the basic volcanic-tectonic systems that led to the development of the Faroe Islands.

Acknowledgements

References

Barth-Wirsching, U. & Höller, H. 1989: Experimental studies on zeolite formation conditions. The European Journal of Mineralogy **1**, 498–506.

Betz, V. 1981: Zeolites from Iceland and the Faroes. Mineralogical Record **12**, 5–26.

Breck, D.W. 1974: Zeolite Molecular Sieves: Structure, Chemistry and Use. New York: John Wiley.

Brewster D. 1825: A description of Levyne, a new mineral species. Edinburgh Journal of Science **2**, 322–334.

Currie, J. 1905: The minerals of the Faroes, arranged topographically. Transactions of the Edinburgh Geological Society (session 1905–1906) **9**, 1–68.

Debes, L.J. 1673: Færoæ et Færoa Reserata. Hafniæ: Suptibus Daniels Paaulli Reg. Bibl. (In Latin and Danish).

Görgey, R. 1910: Ein Beitrag zur topographischen Mineralogie der Färöer. Neues Jahrbuch der Mineralogie und Palaeontologie **XXIX**, 269–315.

Gottardi, G. 1989: The genesis of zeolites. European Journal of Mineralogy **1**, 479–487.

Gottardi, G. & Galli, E. 1985: Natural zeolites. In: Wyllie, P.J., Goresy, A.E., von Engelhard, W. & Hahn, T. (eds): Minerals and Rocks No. 18. Berlin: Springer Verlag.

Hald, N. & Waagstein, R. 1991: The dykes and sills of the early Tertiary Faroe Islands basalt plateau. Transactions of the Royal Society of Edinburgh: Earth Sciences **82**, 373–388.

Jørgensen, O. 1984: Zeolite zones in the basaltic lavas of the Faroe Islands. Annales Societatis Scientiarum Faroensis. Supplementum **9**, 71–91.

Jørgensen, O. 1997: Zeolites and other secondary minerals in cavities and veins, Lopra-1/1A well, Faroe Islands, 1996, 8 pp. + plates. Unpublished Report. Technical studies prepared for Dansk Olie og Gasproduktion A/S 1997 (in archives of the Geological Survey of Denmark and Greenland, GEUS Report file 26129).

Jove, C. & Hacker, B.R. 1997: Experimental investigation of laumontite ® wairakite + H$_2$O; a model diagenetic reaction. American Mineralogist **82**, 781–789.

Kreyszig, E. 1975: Advanced Engineering Mathematics, 707–709, 783–787. New York: John Wiley.

Kristmannsdóttir, H. 1982: Alteration in the IRDP drillhole compared with other drillholes in Iceland. Journal of Geophysical Research **87** (B8), 6525–6531.

Kristmannsdóttir, H. & Tómasson, J. 1978: Zeolite zones in geothermal areas in Iceland. In: Sand, L.B. & Mumpton, F.A. (eds): Natural zeolites, occurrence, properties and use, 277–284. Oxford: Pergamon Press.

Larsen, L.M., Waagstein, R., Pedersen, A.K. & Storey, M. 1999: Trans-Atlantic correlation of Palaeogene volcanic successions in the Faroe Islands and East Greenland. Journal of the Geological Society (London) **156**, 1081–1095.

Liou, J.G. 1971: Stilbite-laumontite equilibrium. Contribution to Mineralogy and Petrology **31**, 171–177.

Miller, I. & Freund, J.E. 1977: Probability and statistics for engineers, 50–63. Englewood, New Jersey: Prentice-Hall.

Neuhoff, P.S., Watt, W.S., Brid, D.K. & Petersen, A.K. 1997: Timing and structural relations of regional zeolite zones in basalts of the East Greenland continental margin. Geology **25**, 803–806.

Noe-Nygaard, A. 1968: On extrusion forms in plateau basalts; shield volcanoes of 'scutulum' type. Science in Iceland **1**, 10–13.

Rasmussen, J. & Noe-Nygaard, A. 1969: Beskrivelse til geologisk kort over Færøerne i målestok 1:50 000. Danmarks Geologiske Undersøgelse I Række **24**, 370 pp. + map vol. (in Danish with summaries in Faroese and English).

Rasmussen, J. & Noe-Nygaard, A. 1970: Geology of the Faroe Islands (pre-Quaternary). Danmarks Geologiske Undersøgelse I Række **25**, 142 pp.

Rumph, B., Reaves, C.M., Orange, V.G. & Robinson, D.L. 1993: Structuring and transfer zones in the Faroe Basin in a regional tectonic context. In: Parker, J.R. (ed.): Petroleum Geology of Northwest Europe: Proceedings of the 4th Conference, 999–1009. London: Geological Society.

Sigurdsson, H. 1967: The Icelandic basalt plateau and the question of SIAL. In: Björnsson, S. (ed.): Iceland and mid-ocean ridges. Societas Scientiarium Islandica **XXXVIII**, 32–46.

Waagstein, R. 1988: Structure, composition and age of the Faroe basalt plateau. In: Morton, A.C. & Parson, L.M. (eds): Early Tertiary Volcanism and the Opening of the NE Atlantic. Geological Society (London) Special Publication **29**, 225–238.

Waagstein, R. & Hald, N. 1984: Structure and petrography of a 660 m lava sequence from the Vestmanna-1 drillhole. In: Berthelsen, O., Noe-Nygaard, A. & Rasmussen, J. (eds): The Deep Drilling Project 1980–1981 in the Faroe Islands. Føroya Fródskaparfelag, Tórshavn, 39–65.

Walker, G.P.L. 1960: Zeolite zones and dike distribution in relation to the structure of the basalts of Eastern Iceland. Journal of Geology **68**, 515–528.

Walker, G.P.L. 1970: The distribution of amygdale minerals in Mull and Morvern (Western Scotland). In: Murty, T.V.V.G.R.K. & Rao, S. (eds): Studies in Earth Sciences, West Commemoration Volume, 181–194. Faridibad, India: Today & Tomorrow's Publishers.

Appendix A: Locations of sites along the sections discussed in the paper and minerals found in vesicles and fractures at each locality. The mineral zones are defined in Fig. 2

Profile	Locality	Altitude (m)	Vesicles	Fractures	Zone
SU1	Road exposure 0.5 km north of Lopranseiði	25	No vesicles.	He–Me. He–St–Ch. An–Ch. Ca. Qz.	2–3
SU1	The northern entrance of the Sumba tunnel	70	–	He–Me. He–Ch. Me–An. Ca. Ch–An.	2–3
SU1	Road exposure at the W slope of Siglidalur	200	–	Ch–An. Ca.	1–3
SU1	Road exposure at small stream on the W slope of Spinarnir	380	–	Ch–Th*. Op. Qz.	1–2
SU1		288	–	Ch–An. Op. Qz. Ca.	1–2
SU1	Road exposure at Stórá, 1km SE of Spinarnir	340	–	Th*–An. Op. Qz. Ca.	1–2
SU1	Lambaklettur	235	–	As above.	1–2
SU2	Road exposure 3 km E of Øravík	100	Empty vesicles.	Ca. Qz.	1–2
SU2	Road exposure 2.5 km E of Øravík	25	Ce–An. Ch–Me*–Th*.	An. Ca. St.	1–2
SU2	Exposure in Dalsá, 1.5 km W of Øravík	100	An, Me*. Ch. Ca. Cld.	Cld. Qz.	1–2
SU2	Road exposure just north of Høgiklovningur, 2.5 km S of Øravík	250	Ca–An. Ph–Th*.	Cld. Me*.	1–2
SU2	Øraskarð	278	Empty vesicles.	Ca.	1–2
SU2	NW slope of Nónfjall	360	Th*–An–Ch.	Th–Th*–An–Ch.	1–2
SU2	The summit of Nónfjall	427	An–Me* Ca. Qz.	An.	1–2
SU2	Road exposure 0.8 km S of the church in Fámjin	80	Ac. Ch.	Ch. An. Qz.	1–2
SU2	Road exposure 0.5 km S of the church in Fámjin	20	An–Th. Th*–Ch.	An. St. Me*.	1–2
SU5	Høvdatangi, Froðba	0–25	Empty vesicles.	Empty fractures.	–
SU5	Skarvatangi	60	Na–(Th, An). Me–Th. Ch.	Me–Me*. Me–St. Me–An. St–Ch. St*–St.	2–3
SU5	Exposure at the road Froðba–Nakkur	90	An–St. Me–St. Th–St. Th–Me.	Me*–Ch.	2–3
SU5	– do –	130	Na. Ch. Me–Sc. Me–Ch. Th–Ga–Ch.	Na–St*–St. An–Th. St–Ch.	2–3
SU5	– do –	140	An–Th*–Ch.	An–Me. St–Me–St. Me–La, Ch.	2–3
SU5	– do –	250	Me–Me*. Th–Me.	An. He–St. Op, Cld, Ca.	2–3
SU5	Summit of Kambur	483	Ce–He. Me in large acicular crystals like scolecite.	Ce–Me*, Ce–An. He.	2–3
SU9	Hamranes and the southern entrance of the tunnel Hvalba–Sandvík	0–100	He–St. He–Me–Ch. An–Me. Me–Me*–Gy. Me–Gy+Ap.	He–St–Ap. Me*–La. Th–Ch; He–(St, La). He–Ap. He–La. La–Ca. La–Gy.	2–3
SU9	The southern slope of Skálafjall	70	An–He. Me–Th. Cld.	As in the vesicles.	2–3
SU9	– do –	120	As above.		2–3
SU9	– do –	160	Scolecite-like Me. An–He. Me–He.	He–Me–Me*. Ca.	2–3
SU9	– do –	200	As above.		2–3
SU9	– do –	240	Me–St. He–St. He–Ch.	Ca–(Ch, Le).	2–3
SU9	– do –	260	Me–Me*–Ch. Th–Ch.		2–3

Profile	Locality	Altitude (m)	Vesicles	Fractures	Zone
SU9	The southern slope of Skálafjall	290	Th*–Ch. Me–Me*–Ch. Ca.		1–3
SU9	The summit of Skálafjall	374	As above.		1–3
SA1	Exposure at the cost line and at road cuttings in Søltuvík	0–50	Many empty vesicles. He. St. La. Ca.	La–St–Ca. Mo–He–St. Ca.	2–4
SA1	Road exposure at the road Sandur–Søltuvík, 1.5 km west of Sandur	60	He–St. He+Me–St. Th–St.	He+Me–St. Ca.	2–4
SA1	Large quarry at lake Sandvatn, 1 km north of Sandur	10	No vesicles.	St–La–Ca. He. St.	2–4
SA1	Sprutthol, Sandsvágur Bay	30	He–Me. Ch. Ca.	St. Ca.	2–4
SA3	Húsavíklið N of Húsavík	0–75	He–Me. Ce–Me. Th–Me.	St.	2–3
SA3	Road exposure 2 km W of Skálavík	78	Me–Ch. Gi. Cld.	He–St–Ca.	2–3
SA3	Road exposure at Hálsur, 3 km W of Skálavík	119	Me–Th. Me–Me*. He–Th.	St–St*. Ap.	2–3
SA3	Urðarklettar NW of Húsavík	120	Me–Th–Ch. An–Me–Th.		2–3
SA3	Húsavíklið N of Húsavík	150	Me–Th–Me. An. He. Ca.		2–3
SA3	Exposure at Gravaráin	140	Me–Th. He–St. He–Ch. An.	St. La.	2–3
SA3	Urðatklettar, NW of Húsavík	150	Ce–Me–Th–Me*, Me–Me*–Gy.	Me*.	2–3
SA3	– do –	180	Ca–Me–Me*. An–Me.		2–3
SA3	Húsavíklið, N of Húsavík	180–200	Me–Th*. An–Th–Me*.		2–3
SA3	Exposure at Gravaráin	210–220	Me–Ca–. Me*. An–Me*. An–Th*.	Ca–He–St. Ca–Ap.	1–2
SA3	Exposure at Stórá	243	Me–Me*. Me–Th*–Ca. Gi.	Ca–St.	1–2
SA3	Summit of Heiðafjall	266	He–Me*. An–Me*–An. Th*.		1–2
SA3	Exposure at Stórá	320–340	Me–An–Me*. Ch. Th*.		1–2
SA3	Skriðubakki	360–380	Th*–Ch. Me*–Ch.	Me*.	1–2
SA3	– do –	400–420	Ch–Th*. Th*–Ch. An. Many empty vesicles.		0–1
SA3	The summit of Pætursfjæll	447	Ch–Th*. Many empty vesicles.		0–1
SA5	Dalsnípa	150	Me–An. Me–Ap–St. Th–Ap. Ch–Ap. Th–Ch. An–Ch.	Le. He–St–Ap. Cld.	2–3
SA5	The S slope of Skúvoyafjall, 0.6 km NW of Dalsnipa	280	Me–St, Me–An, He.		2–3
SA5	The summit of Skúvoyafjall	354	Ce–Ch. Ce–Th–Th*.	St.	1–3
SA5	Road exposure at the end of the road Dalur–Skuvoyafjall	308	He–Me. Th–Me*. Ch–Th*.		1–3
SA5	Road exposure 2 km SW of Dalur	260	Th–Ap. St–Me–Le. Th–Le.	He–Me–La.	2–3
SA5	Dalur harbour	0–30	Ch. Ch–Le. An–Th–Th*. He–Me–St.	Ch. Le. Me–Ap–St. Me–Me*.	2–3
SA5	Road exposure at Kinnartangi	100	Ch. Ch–Th–Ch. St–Me–Gy. Gy–Me.		2–3
SA5	The SE slope of Stórafjall	160	Ch. An–Me–Me*. St–Th.	Ch. St. He. Gy.	2–3
SA5	– do –	220	Me–Me*–Ch. Th–Me.		2–3
SA5	– do –	260	As above.		2–3
SA5	– do –	300	Ph. Gi–Me*. Th*–Le. Me–Me*.		1–2
SA5	– do –	340	As above.	Ch–Le. He–Me–St–Ap.	1–2
SA5	– do –	360	As above.	He–Le.	1–2

Profile	Locality	Altitude (m)	Vesicles	Fractures	Zone
SA5	The summit of Stórafjall	396	Ch+Ph. Gi–Me*. Me*–Ch. Th–Ch.		1–2
SA5	The NE slope of Stórafjall	310	Ch. Me*–Ch. He.		1–2
SA5	Trigonometric station on the NE slope of Stórafjall	217	Ch. An. Me–Ch. He–St. He–Me–Gy.		2–3
SA5	Road exposure at Tjarnaheyggjur	60	As above.	Me–Ca.	2–3
VÁ1	Reyðastiggajatangi	0–10	He–St, An.	Cl–St–Ca–La.	3–4
VÁ1	Gásadalur, exposure along the path Gásadalur–Rógvukollur	100	He–St, St–La.	Cl–St–La.	3–4
VÁ1	– do –	200	He, St.	Me, La, An.	3–4
VÁ1	Gásadalur, exposure at the path Gásadalur–Rógvukollur	235	He–Th.	La, Ca.	3–4
VÁ1	Gásadalur. The pass between Knúkarnir–Neytaskarð	340	He, St, Th, An, Cl.		3–4
VÁ1	Grunnadalur, exposure at the branching of small streams	380	Cl–He–Th, Cl–He–St, Cl–St–Me.	St–La–St.	3–4
VÁ1	Rógvukollur , exposure at the W slope	380	He–Me, Me–Ch, Th–Ch–Th, Mo–He, Mo–Ch ± Cld.	Me, Ca.	2–3
VÁ1	Neytaskarð, exposure at the SE slope	400–420	As above.		2–3
VÁ1	The summit of Rógvukollur	464	He–Me, Me–He–Me, Th–Me, Th–Ch, Me–Ch.		2–3
VÁ1	Djúpidalur (the NW slope of Eysturtindur), exposure at stream	470–480	He–Me, He–Ch, Me–Ch, Th–Ch.		2–3
VÁ1		500	He, Me, Th, Ch.		2–3
VÁ1	Grunnadalur, exposure at the end of small streams	550	Th–Me*–Ch.	La, Ca.	2–3
VÁ1	Djúpidalur (the NW slope of Eysturtindur)	600–610	Ce–Th–Th, Ce–Ch.	St–Me–La, Ca.	2–3
VÁ1	The plateau between Eysturtindur and Akranesskarð	620–640	An, Th, Me, Sm.		2–3
VÁ4	Oyrargjógv ferry harbour and the path to Sørvágur	0–136	St–St*. Ep–St. La. Th. Ch.	St. La.	3–4
VÁ4	Large quarry 1 km W of Sørvágur	10	Cl–St–St*. St–La. Mo–He. Mo–Gy. An–Gy. Me–Me*–Ch. Me–Ap±Sm.	He–St–St*. Ep. La, Me.	3–4
VÁ4	Sjatlá, 1.5 km N of Sørvágsvatn	45–60	Cl–He–St. St–La. Ap.		2–4
VÁ4	Exposure at N end of small road from Sørvágur, just W of Sjatlá	114	Cl–St–Me. Cl–An. Cl–Ch±Sm.	St–La. Ap.	2–4
VÁ4	– do –, exposure at small tributary of Skjatlá	150	Cl–He–St. St–Ap. Cl–Me–Th. Cl–Me–Ch. Me–Ap. Me–Ch.	Me–Ap. An–Ap. He–Ch.	3–4
VÁ4	– do –	190	As above.		3–4
VÁ4	– do –	220	Cl–St–St*. Cl–He ± La. Th.	Mo–St.	3–4
VÁ4	End of Breiðá (Oyrargjógv)	250	Ce–Me. He–Me.		3–4
VÁ4	– do –	304	Ce–Me–Th. Ce–Th–Ch.	Gy–Me.	2–3
VÁ4	Kvígandalur, exposure at the SE tributary of Kvígandalsá	250	An. He–Le. Me–Le. An–Th–Ch.		2–3
VÁ4	Husadalur, exposure at the W? tributary of Kirjuá	275	An. Me. He.	Me–An.	2–3

Profile	Locality	Altitude (m)	Vesicles	Fractures	Zone
VÁ4	Kvígandalur, exposure at the SE tributary of Kvígandalsá	300–365	An. He. Le. Ch.		2–3
VÁ4	The cross between the path Oyrargjógv–Sørvágur and Sandavágur–Slættanes	436	Me. Th. St. Ch.		2–3
VÁ7	Road exposure 3 km north of Sandavágur	100–120	Ce–He–St. Ce–St–Me. Ce–He–Th. Ce–Mo–St. Ce–Me–St.	Ce–Mo–He. Ce–He–St. Ce–Me*–Ch. Ce–Ap.	2–4
VÁ7	The western slope of Malinstindur	219	As above.		2–4
VÁ7	– do –	235	Ce–He–Me. Ce–Me–Gy.	St–Ca.	2–3
VÁ7	– do –	280	Ce–Me–Ch.±Ca. ±Sm.		2–3
VÁ7	– do –	345	As above.		2–3
VÁ7	– do –	386	Empty vesicles.		–
VÁ7	– do –	410	Ce–He–Me. Th–Me. Th–An.	St. Ch.	2–3
VÁ7	– do –	500	As above.		2–3
VÁ7	– do –	538	He. An. Me. Th. Th*. Cld. Ca.	He–Me. Me*. Cld.	1–2
VÁ7	– do –	563	Me–Me*. Th*–Ph. Th*–Ch+Le.		1–2
VÁ7	The summit of Malinstindur	580	Ce–Me*.		1–2
VÁ7	– do –	620	He. Me. Ph. Ch. Th.	Ca. Cld.	1–2
VÁ7	– do –	683	Me–He. Me*–Ch. Ph–Ch.		1–2
VÁ7	– do –	690	He. Ch. Le. Th. Cld.		1–2
ST2W	The path Saksun–Haldarsvík: Kvíggjarhamar, Saksun	0–100	He. St. Th. Me. Ch.	St–Ca–St. Gy. Tb. Ok.	2–3
ST2W	The slope of the mountain between Skipá and Gellingará	150	He–Ch–Th. Me–St.		2–3
ST2W	– do –	200	Me. Ca.		2–3
ST2W	– do –	250	Th–Me. He–Me. Me–Ch.	St. La.	2–3
ST2W	– do –	310	As above.		2–3
ST2W	– do –	325	Me. Me*. Th*–Ch. He–Me.	Ok. Gy. Ca.	2–3
ST2W	– do –	355	Me–Me*. Th–Me*. Th*–Ch.		2–3
ST2W	– do –	360	Ce–Th*. He–Me*–Sm.		1–2
ST2W	– do –	380	An–Th*. Th*–Le.	Me*–Ca.	1–2
ST2W	– do –	407	Ce–Ph–Ch. Ce–Th*–Ch.		1–2
ST2W	– do –	430	Th*–Ch.		1–2
ST2W	– do –	460	Empty vesicles.		0–1
ST2W	– do –	555	Le–Ch. Th–Th*.		0–1
ST2W	Víkarskarð	600	Ce. Th. Ch. Cld.		0–1
ST2W	The NE slope of Gívrufelli	650	As above.		0–1
ST2W	The summit of Gívrufelli	701	As above.		0–1
ST2E	Víkarnes N of Haldarsvík	0–30	He–St. Ca.	Ca–La.	3–4
ST2E	The SE slope of Fjallið	100	As above + Th. Gy. Ok.	To–Gy. La.	3–4
ST2E	– do –	150	He. Me. Th.	To–St. Th–Gy–Ap.	2–3
ST2E	The summit of Fjallið	180	He–Me. He–Th*. Ca.		2–3

Profile	Locality	Altitude (m)	Vesicles	Fractures	Zone
ST2E	The path Haldarsvík–Saksun: exposure 0.5 km SW of Haldarsvík	148	He–St. Me.	Me–Th–Ch. Me–An. Ph–Le–Ch.	2–3
ST2E	– do –, exposure 1 km SW of Haldarsvík	200	He–St. He–Me.		2–3
ST2E	– do –, exposure at the Svínstiáir tributaries of Kluftá, 1 km SW of Haldarsvík	230	Me. Th. He.	St. Ca.	2–3
ST2E	– do –, exposure 1.2 km SW of Haldarsvík	250	He. Me. Mo.	He. St. Ap. Ca.	2–3
ST2E	– do –, exposure 1.5 km SW of Haldarsvík	280	Me–Th–Me–Gy–Sm.		2–3
ST2E	– do –, exposure 1.8 km SW of Haldarsvík	350	Me–Th.		2–3
ST2E	– do –, exposure 2 km SW of Haldarsvík	360	Me–Th. Me–Ph–Ch.		2–3
ST2E	– do –, exposure 2.3 km SW of Haldarsvík	370	Me–Th. An–Me–Me*.		2–3
ST2E	– do –, exposure 2.5 km SW of Haldarsvík	400	Th*–Ch. Me–Th*.	Ph–Ch. Ch + Le.	1–2
ST2E	– do –	410	Me–Me*. Ch–Le–Ch.		1–2
ST2E	The SE slope of Víkartindur	420	Me–Me*–Le. Ch–Ph–Sm.		1–2
ST2E	– do –	440	.Me*. Th–Th*–Ch.		1–2
ST2E	– do –	500	Th*. Ch.Cld.		0–1
ST2E	– do –	540	As above.		0–1
ST2E	– do –	620	As above.		0–1
ST6W	Road exposure at the main road Kvívík–Stykkið, 1.5 km E of Kvívík	50	He. St. La. Me. Th. Ap.	He. St. Ap. Me*. Th. Ch. An.	2–4
ST6W	Tunnel workplace at the village of Leynar	50	Me. St. La.		2–4
ST6W	Exposure at Leynarvatn along the old road Tórshavn-Vestmanna	60–125	He. St. Wa. La. Ce. Cld.	St. Ca. He. St. St*. La. Me*, Th, Le.	2–4
ST6W	The path Leynarvatn–Hósvík, exposure 0.3 km NE of Leynarvatn	150–190	Ce–He–St. Ce–Me–Gy. Cld.	Ph, Gy, Ap.	2–3
ST6W	– do –, 0.4 km NE of Leynarvatn	210	Ce–He–St. Ce–Me–Th. Ce–St–La.		2–3
ST6W	– do –, 0.5 km NE of Leynarvatn	260	Ce–Me–Th. Ce–He–Me. Ce–He–Th.	Me–Ca.	2–3
ST6W	The path Leynarvatn–Hósvík, exposure 0.5 km NE of Leynarvatn	300	As above.		2–3
ST6W	– do –, 0.6 km NE of Leynarvatn	340	As above.		2–3
ST6W	á Halsi, 1 km NE of Leynarvatn	380	As above.		2–3
ST6W	– do –, 1.5 km NE of Leynarvatn	463	Ce–He–Me–Me*. Ce–Th–Ch.		2–3
ST6W	– do –, 1.9 km NE of Leynarvatn	500	As above.		2–3
ST6W	– do –, 2 km NE of Leynarvatn	510	Me–He–Me*. Me–Me*. Th*–Ch.	He–Me.	2–3
ST6W	Hósvíksskarð	520–530	Th. Th*. Ph. Ch. Le. + Ce.		2–3
ST6W	The SW slope of Bøllufjall	550	As above.		1–2
ST6W	The summit of Bøllufjall	584	As above.		1–2
ST6W	The SW slope of Gívrufjall	530	As above.		1–2
ST6E	Road exps. between við Áir and Hosvík	15	He–St*. He–St–Ap. He–St–Ch. He–Th–Ch. Th–St. Th–Ch. Ga–Th. An–Ch. An–Ap. An–Th. An–Th–Ch±Ce.	He–Ch–St. Th–Gy+Ap. Ch–Th*–Ap.	2–3
ST6E	The path Hosvík–Leynar: Smørdalsá	160–203	He–Me. He–Ch–Th, Me–Gy. He–An–Th.		2–3

Profile	Locality	Altitude (m)	Vesicles	Fractures	Zone
ST6E	The path Hosvík–Leynar: Smørdalsá	240–260	Ce–Me–He. Ce–Th–Me. Cld.	Me–Th–Ap–Gy.	2–3
ST6E	– do –	360	As above.	Ca–La. Cld.	2–3
ST6E	The NE slope between Bøllufjall and Gívrufjall	436	Me–Th. He–Me–Ca. He–Th.		2–3
ST6E	– do –	480	He–Me–Me*. Th–Ch. Th–Th*.		2–3
ST6E	– do –	500	Th–Th*–Gy. Me*–Gy.		2–3
ST6E	The NE slope of Bøllufjall	530	Th–Th*. Th–Ph, Th*–Ch.		1–2
ST6E	The summit of Bøllufjall	584	As above.		1–2
ST10	Large quarry 0.5–1 km NW of Sund, Kalsbaksfjørður	15	Me. Me*. Th. An. Ph. Gi. Ap.		2–3
ST10	Exposure at Sundá, 1.2 km S of Sund	227	He. Me. Ca.		2–3
ST10	– do –, 1.6 km SW of Sund	265	Me. Th.	St–He.	2–3
ST10	Quarry 0.5 km SW of Lambafelli at the high road Tórshavn–Kollafjørður	340	Ce–He. Ce–Ch–Le. Ce–An. Ce–Ch.	Ce–He–Sm, Ce–He–Ch. Ce–He–Th–Ch.	2–3
ST10	Road exps. 1 km W of Sundshálsur along the high road Tórshavn–Kollafjørður	310	Ce–He–Me. Ce–Me–Ch. Ce–Th–Me.		2–3
ST10	Small quarry at end of road to the water reservoir of Havnardalur	170	He. Me. Th. Ch.		2–3
ST10	Road exposure at the road Tórshavn–Velbastaður, 0.5 km N of Velbastaður	160	Ce–Me. Ce–Th–Ch.		2–3
ST10	Exposure at the road Tórshavn–Velbastaður, just N of Velbasta ur	123	Me–Me*. Me–Ch. Me. Th–Ch. Th–Me–Me*.	Cld, Ca.	2–3
EY1	Road exposure at the road Eiði–Norðskáli, 0.4–0.5 km SE of Eiði	60–100	Ap–Gy–Me. Me–Ph. He–Gy–Me. He–Me–Ch. St–Aå–Sm. Th–Ap. Th–St–Ap. Th–Ch–Sm.	St–La–St*–Ca. He–St– Ch–Sm.	3–4
EY1	Localities on the road Eiði–Funningur: Quarry in Djúpidalur, 2 km east of Eiði	150	St–Gy. St–Th–Gy. Th–Ga–Th. Me–Th. Me–Ch.	St–La.	3–4
EY1	50 m long road cutting on W slope of Slættaratindur, 3.5 km east of Eiði	200–230	Me–Th*–Gy. Me–Th*–Ch. Me–He–Me. He–Me.	St–St*. La–Me*–Sm. He–Ap. St. Cld. Qz.	2–3
EY1	Road exposure 0.4–0.5 km E of Eiðisskarð just at the N slope of Vaðhorn	336–346	Ce–Me–Th*. Ce–Me–Ch.		2–3
EY1	The N slope of Vaðhorn	410	As above.	He–St–St*. Mo–St.	2–3
EY1	– do –	435	As above.		2–3
EY1	Small quarry at the road fork Eiði, Funningur, Gjógv, 1 km west of Funningur (165)	165	He. St. Me. Me*. Ch.		2–4
EY1	Exposure at the coast line at Funningur	5–10	Mo. He. St. Me. +Ce.	St. An. Me. Cld.	3–4
EY2	Exposure at the coast between Stórá and Marká	0–20	Mo. He. St.	St. Qz. Cld. Ca.	3–4
EY2	The path Svínár–Funningur	30–40	He–Me. He–St–Gy. He–Me–Gy.		3–4
EY2	– do –	100	Me–Th–Ch. Th–Gi. Th–Me*. An–Ch. An–Th–Ch.	Th–Gy–Ap. Me–Ap–St.	2–3
EY2	– do –	212	As above.		2–3
EY2	– do –	280	Me. Th. An. Ch.	An–Th*–Gy.	2–3
EY2	– do –	346	An. Me. Me*. Th. Th*. Th–Ch–Sm.		2–3
EY2	– do –	400	Ce–Th–Th*–Ch. Ce–Ch.	Th–Th*–Ch.	1–2
EY2	– do –	420	Ch–An. Ch. Gi–Th*. An–Ph–Ch.		1–2

Profile	Locality	Altitude (m)	Vesicles	Fractures	Zone
EY2	Kvígandalsskarð	460	Me*. Th*. Ch. Gy. Sm.		1–2
EY2	– do –	480	As above.		1–2
EY2	The E slope of Skerðingur	500	As above.		1–2
EY2	– do –	525	As above.		1–2
EY2	– do –	450	Ce–Th*. Ce–Me–Me*–Ch.		1–2
EY2	– do –	430	As above.		2–3
EY2	– do –	415	Ce–An. Ce–Qz. Cld.		2–3
EY2	– do –	380	Me.		2–3
EY2	Kvígandalur	363	He–Me. He–Th.		
EY2	Skipagjógv	180	Me–Th–Th*. Ch–Gi–Th.	An–Th–Ap–Gy–Sm. Cl. Ca.	2–3
EY2	– do –	80	He. Me. Th.	Ca.	2–3
EY2	– do –	50	Gy–He. Gy–Th–Me.		3–4
EY2	Skipagjósoyran	0–10	He. St. Th. La. Gy.	He. Me–La–St.	3–4
EY3	Large quarry 1 km S of Oyri	20–30	Me–Th–Sm. Me–Th–Ch–Sm. Me–Gy–Me*.	Cl–He–Th–Ap.	2–3
EY3	Oyrargjógv	100	Me–Th, Me–Gy.		2–3
EY3	– do –	210	No vesicles.	He. St. Me. Th. Gy.	2–3
EY3	The path Oyri–Skálafjørður	251	Me. Th. Ch.		2–3
EY3	– do –	300	He–Me. Th–Me. Th–Ch.		2–3
EY3	– do –	340	An. Me*–Ch.		1–2
EY3	– do –	350	Me*–Ch. Th–Th*.		1–2
EY3	– do –	400	Th–St–Gy. Ch. St.		1–2
EY3	– do –	426	An–Th*. An–Th*–Ca. Ch.		1–2
EY3	– do –	495	Th*–Ch+Le.		1–2
EY3	The SW slope of Sandfelli	527	Ce–Th*–Ch. Ce–Cld.	He. Me. Ca. Cld.	0–1
EY3	– do –	545	As above.	As above.	0–1
EY3	The summit of Sandfelli	572	As above.	As above.	0–1
EY3	The path on the S slope of Skálafjall	440	Me–Th. He–Me.		2–3
EY3	– do –	405	As above.		2–3
EY3	– do –, just at Öksnagjógv	200	As above.		2–3
EY4	Small quarry just N of Morskarnes, about 1 km N of Nesá	20	He–Th–Ch. Me–Th.	He–St. He–Ap. Ca.	2–3
EY4	The W slope of Neshagi, just E of the locality above	140	Cl–Me–Th. He–Th.		2–3
EY4	Exposure at Skotá	194	As above.		2–3
EY4	– do –	230	Me–Me*. Ch.		1–2
EY4	– do –	320	Th*. Me–Me*. Ch.	He–Me. He–St.	1–2
EY4	The SE slope of Kambur: exposure between the source of Skotá and Urðará	380	Me*. Ch, Le +Ce.		1–2

Profile	Locality	Altitude (m)	Vesicles	Fractures	Zone
EY4	The SE slope of Kambur: exposure between the source of Skotá and Urðará	400	As above.		1–2
EY4	– do –	430	Th*. Ch. Le. Ce.		0–1
EY4	– do –	462	Ch. Many empty vesicles.		0–1
EY4	The path Steffanstangi–Kambur	480	As above.		0–1
EY4	– do –	500	Th–Ch–Th*. Cld. Ca.		0–1
EY4	– do –	540	As above.		0–1
EY4	The summit of Kambur (trigonometric station)	593	As above.		0–1
EY4	The E slope of Heygshagi	440	Me*–Ch. Th*–Ch.		1–2
EY4	– do –	400	As above.		1–2
EY4	– do –	250	As above.		1–2
EY4	Markrá	250	Me–Me*. He–Th. He–Me*.		2–3
EY4	– do –	160	As above.		2–3
EY8	Road exposure at the old road Lervík–Fuglafjørður/Norðragøta, about 2 km NW of Lervík	80	Ce–Mo–He–Me. Ce–Ch.	He–Me–St.	2–3
EY8	Localities along Kálvadalsá in Kálvadalur	200	Mo–He–Me–Me*. An–Th–Ch. Le–Ch–Le.	He–Me–St–St*. An–Th.	2–3
EY8	– do –	270	As above.		2–3
EY8	– do –	300	He–Me*–Ch. An–Th*–Ch.		2–3
EY8	Mannsgjógv	400	An–Ph–Ch. An–Th–Ch, Me*–An.		1–2
EY8	The NE slope of Navirnar	300	He–Me–St*. He–Ch, He–Le. An–He.	He–St. He–Me.	2–3
EY8	The E slope of Ritafjall	440	He–Me*–Ch. An–Th*–Ch.		1–2
EY8	– do –	490	He–Th–Ch. Me*–St*.		1–2
EY8	– do –	520	Th–Ch. Me*–Ch.	He. St. Ca.	0–1
EY8	The summit of Ritafjall	560	Th. Ch. Le.		0–1
EY8	– do –	641	Th*. Nearly all vesicles are empty.		0–1
EY10	Large quarry just N of the road fork Skálafjørður–Runavík–Lambi	60–80	Me–St*. Th–St*. Th–Me–An. Th–Ch–St*. Co–Th. Ha.	He–St*. He–Th–Ca. Ph–Ch–Ph. Ha–Ca.	2–3
EY10	The SW slope of Ritafelli, NE of the locality above	180	No vesicles.	He–Me–Ch–Sm. Me*–Le–Ch–Sm. An–Me*–Sm.	2–3
EY10	– do –	200	Me–Me*. Ch. Th*. Ph.	An–Me*–Sm. Me*–Ph–Le. Ap–Sm.	1–2
EY10	– do –	230–240	As above.		1–2
EY10	– do –	270	He–Th–Ch. Th*–Ph. An–Th*, Ch–St. An–St. Ap–Th–Ph. Ca.	St–La. Me–Ap.	1–2
EY10	The edge of Ritafelli	350	St, Me*. Th*. Ph. Ch. Ce.		1–2
EY10	The SW slope of Stórafjall	380	Th*. Ch. Ph.		1–2
EY10	The W edge of Stórafjall	440	Th. Ph. Ch. An. Ce.	An. St. Ch. Ph. Sm.	0–1
EY10	– do –	490	Empty vesicles.	St, Th*. Ch. Ca. Cld. Sm.	0–1

Profile	Locality	Altitude (m)	Vesicles	Fractures	Zone
EY10	The W edge of Stórafjall	520	Th. Many empty vesicles.		0–1
EY10	The summit of Stórafjall	567	As above.		0–1
BO1	Large quarries at Klakkur	60	Me–Ch. He–Me. Cld.	Mo–St–La. Ca–St.	2–3
BO1	The NE slope of Klakkur	100	Mo–An. Mo–He. Me–Ch. Ca.		2–3
BO1	– do –	140	Me–Th*. Ga–Me. Ch–Gi–Th.	As in the vesicles.	2–3
BO1	The NE slope of Klakkur	160	Th–Me*–Ph. Ph–Ch.	He–St. Ca–St.	1–2
BO1	– do –	210	Mo–He–Ch. Ch–Th. Th–Ph. Le–Ch.	Ca–St.	1–2
BO1	– do –	260	Me–Th–La. An–St–La. An–Th–Ch.		2–3
BO1	The summit of Klakkur	414	Ch–Th. Th–Ph.		2–3
BO1	The S slope of Klakkur	380	As above.		2–3
BO1	– do –	300	Me–Th. Th*–Ch. Th–Ph–Ch.	He–St–La.	2–3
BO1	– do –	260	He–Me–Th. He–Th.		2–3
BO1	The NE slope of Hálgafelli	280	Ce–He–Me–St. Ce–Me–An.		2–3
BO1	– do –	300	As above.		2–3
BO1	– do –	360	As above.		2–3
BO1	– do –	380	Ce–Mo–He–Th. Ce–He–Me.		2–3
BO1	– do –	400	Ce–St–Ch.	He–Th–Me–St.	2–3
BO1	– do –	450	As above.		2–3
BO1	– do –	480	An–Me–Me*. Th–Ch.		2–3
BO1	The summit of Hálgafelli	503	Ce–He–Me.	St–La.	2–3
BO2	Exposure at stream 0.6 km SW of Norðoyri	20–80	He. Me. Ch. An. Ap.	St. Cld. Ca.	2–3
BO2	The W slope of Høgahædd	140	An. Me. Ch. Many empty vesicles.	As above.	1–3
BO2	– do –	220	He–St. He–Ch–St. Th–Ph.	St. Ca.	2–4
BO2	– do –	270	Empty vesicles.		–
BO2	– do –	310	He–Me–Me*. Me–An. Me–Ch.		2–3
BO2	– do –	320	Ch–Th*–Ch. He–Ch. Th*. An.		1–2
BO2	– do –	330	Me*. Th'. Ch. Ca.		1–2
BO2	– do –	360	As above.	Ch. Th*. Ca.	1–2
BO2	– do –	440	Th*. Ca. Op.	Cld.	1–2
BO2	– do –	474	Me. Me*. Th*. Ch.		1–2
BO2	– do –	510	Th–Th*. Ca. Cld. Many empty vesicles.		0–1
BO2	– do –	550	As above.		0–1
BO2	The summit of Høgahædd	563	As above.		0–1
BO3	Large quarry between Norðdepil and Depil	40–50	Ce–He–Th. Ce–He–Na–Th. Ce–Th–Ch.	Cl–He–St–Ap. Cl–Th–Ap. Cl–Ph.	2–4
BO3	Depilsá	150	Me–Me*–Ch–Le. Me–Me*–Ch. He–Me.		2–3
BO3	– do –	200	Me*–Ch, An–Ch.		1–2
BO3	– do –	300	He–Me*–Ch. He–Th*–Ch. An–Ph–Ch. +Ce.	He–St. He–Th–Ca.	1–2

Profile	Locality	Altitude (m)	Vesicles	Fractures	Zone
BO3	Depilsá	340	As above.		1–2
BO3	E slope of Lokki	375	Ch–Gi–Th'. Ch–An.		0–1
BO3	– do –	400	Ch–Th*–Ch. Ch–Le.		0–1
BO3	– do –	450	As above.		0–1
BO3	– do –	470	Th. Ch. Ca.	He–St–Th–Ca.	0–1
BO3	E slope of Lokkanøv	460	Ce–An–Ch. Ce–Th–Ch–Th*. Many empty vesicles.		0–1
BO3	– do –	580	As above.		0–1
BO3	– do –	700	As above.		0–1
BO3	The summit of Lokki (trigonometric station)	754	As above.		0–1
VI1	The starting point of the profile is the largest stream 0.5 km SE of Hvannasund	50	Ce–Me–St. Ce–An–Th–Me. Ce–Me–Ch. Ce–He–St–Me.	Ce–Cl–St. Ce–Cl–Me–Ca.	2–3
VI1	SW slope of Enni	120–132	Empty vesicles.		–
VI1	SW slope of Enni	180	Mo–An.		2–3
VI1	– do –	210	An. Ph–Ch. An–Th. Me–Me*. He–Me–Ch.	He–Me*–Ch. He–Ph–Ch. He–Th–Me.	2–3
VI1	– do –	225	As above.		1–2
VI1	– do –	240	Me*. Th*. An.		1–2
VI1	– do –	270	Ce–Th–Th*–Ch. Ce–Ch–Le. Ce–An–Ch. Ce–Ch–St. Ce–He. Ce–He–Cld.	He–St. Cld.	1–2
VI1	– do –	310	Ch–Gi–Th*. St–Ch. Ph–Ch. Th–Th*.		1–2
VI1	– do –	360	Ce–Ch. Ce–Ph–Ch. Ce–Th*. Ch.		1–2
VI1	– do –	380	Ch. Th. Le. Sm.	Cld.	1–2
VI1	– do –	420	Th*–Le–Ch–Sm.	Op. Sm.	0–1
VI1	– do –	550	As above. Many empty vesicles.		0–1
VI1	– do –	600	Ca and Siderite.		0–1
VI1	The summit of Enni	651	As above.		0–1
VI2	Small quarry at the road Hvannasund–Viðareiði, 2.6 km N of Hvannasund	40–80	Ce–He–Me. Ce–He–Th. Ce–He–Ch–Sm. Ce–Ch–Sm. Ce–Ph–Me*. Ce–Me–Me*.	He–Me–St.	2–3
VI2	W slope of Tunnafjall	80–100	He–Me–Me*. An–Th–Me. An–Th–Ch. An–Ph–Ch.	He–St. St–Me.	2–3
VI2	– do –	150	As above.		1–2
VI2	– do –	200	As above.		1–2
VI2	– do –	225	Me*. Th*. Ch. Ph. An.	He. St. Ca.	1–2
VI2	– do –	250	Me*. Th*. Ch.		1–2
VI2	– do –	300	Th*. Ch.		1–2
VI2	– do –	315	As above.		0–1
VI2	– do –	390	An. Th'. Ch. Ph.	Me*. Ph. St.	0–1
VI2	– do –	460	Th*. Ch. Le. Sm.	St. Sm.	0–1
VI2	– do –	520–550	Empty vesicles.	Qz. Cld. Ca.	0–1

Profile	Locality	Altitude (m)	Vesicles	Fractures	Zone
VI2	The summit of Tunnafjall	593	Th. Th*. Ch.		0–1
VI2	The S Slope of Myrnafjall	620	No vesicles.	Th. Th*.	0–1
VI2	The summit of Myrnafjall (trigonometric station)	688	Th. Th*. Only 20% of the vesicles are mineralised.		0–1
VI3	Small quarry at the road Viðareiði–Hvannasund, 2.5 km south of Viðareiði	80	He–Th*. Me–Me*–Ch–Se.	As in the vesicles.	1–2
VI3	The W and the SW slope of Malinsfjall	150	He–Th*. Me–Me*–Ch. An–Me*–Ph.		1–2
VI3	– do –	200–220	Th*. Ch. Le.	Me. Me*. Th. Th*. An. St.	0–1
VI3	– do –	255	Th*. Ph. An.	He–St.	1–2
VI3	The W and the SW slope of Malinsfjall	310	Th*–Ch.		0–1
VI3	– do –	300–330	Me–Th*. Gi–Ch.		0–2
VI3	– do –	440	Th*. Ch. About 50% of the vesicles are empty.	An–St.	0–1
VI3	– do –	540	As above.		0–1
VI3	– do –	605	Ch–Th–Le. Ca.	Ca–Th–Ca.	0–1
VI3	– do –	660	All vesicles are empty.		0–1
VI3	– do –	680	As above		0–1
VI3	– do –	710	Scattered mineralisations of Th and Ch.		0–1
VI3	The summit of Malinsfjall	750	As above.		0–1

Appendix B. Minerals found in vesicles within different depth intervals in the Lopra-1/1A and Vestmanna-1 boreholes

Max depth	Min depth	Vesicles	Zone
Lopra-1/1A			
−3543	−3400	**La**, Pr, Ca, Cl.	HT
−3400	−3200	**La, Mo**, Pr, Cl.	HT
−3200	−3000	**La, Mo**, Pr, Sm, Qz.	HT
−3000	−2800	**La**, Pu, Qz, Cl.	HT
−2800	−2600	(no data)	
−2600	−2400	**La**, Ca, Pr ,Cl.	HT
−2400	−2200	**La**, Pr, Pu.	HT
−2200	−2000	Th, Ep, He, **La**, Pr, Wa, Mo, Ca, Ce, Sm, Cl, Si.	5–6
−2000	−1800	Sc, Th, Ep, He, **La,** An, Ca, Ce, Cl, Si.	3–5
−1800	−1600	Sc, Th, **St**, Ep, **La**, An, Ca, Ce, Sm, Cl, Si.	3–5
−1600	−1400	Sc, Th, **St**, Ep, He, **La**, An, Ca, Ce, Sm, Si.	4–5
−1400	−1200	Me, Th, **St, Ep, He**, La, Ce, Sm, Cl, Si.	4–5
−1200	−1000	**Me, Sc, Th, E**p, He, La.	3–4
−1000	−800	**Me, Sc, Th, St, Ep**, He, La, An, Ca, Cl, Si.	3–4
−800	−600	Th, St, **Ep, He**, La, An, Cl.	3–4
−600	−400	Me, **Sc**, Th, Ep, He. An. Ca.	2–3
−400	−200	**Me, Sc**, Th, **Ep**, He, An, Ca, Cl, Si.	2–3
−200	0	**Me, Sc,** Th, **St, He**, An, Mo, Ca, Cl, Si.	2–3
Vestmanna-1			
−600	−575	He. He–Ch.	3–4
−575	−550	He. An. St–St*. Ch–Sm.	3–4
−550	−525	He–Ch. Ap. Th–Ap. Ch–Sm.	3–4
−525	−500	He. He–Ac. Th–Ch. St–Ch.	
−500	−475	An–Th–Mt. Th–Sm.	3–4
−475	−450	An–Th–Sm. Th–Sm.	3–4
−450	−425	Gy–Th–Sm. An. An–Th–Sm. Th. Sm.	3–4
−425	−400	An. He–La–Ch. Me–Ch. Th–Sm. Ch–Sm.	3–4
−400	−375	He–La–Ch. Me–Ap–Ch. Me–Ch+Le–Sm. Ch–Sm.	3–4
−375	−350	Me. Gy–Th–Sm. Th–Sm. Th*–Ch. Ch+Le.	2–4
−350	−325	Ap. Th–Ap. Gy–La. Gy–Th–St. Ph. Th*–Sm. Th*–Ch.	1–4
−325	−300	He. He–Me. He–La–Ch. Mo–He–Ch, Th*–Sm. Th*–Ch, Ch–Sm.	2–4
−300	−275	He. He–Ch. Me–He–St. Th–Ga–Ch. Th*–Ph–Ch. Th*–Ch. Ch–Sm.	2–4
−275	−250	Me. Me–Th–Ch. Me–Th–Ph–Ch.. La–Me. Ap. Th–Ch–Sm. Ch–Sm.	2–4
−250	−225	Th–Gy–Sm. Th–Th*–Ch. He–Th–Ap. Le–Sm.	2–4
−225	−200		
−200	−175	He. He–Ch–Ap–Sm. Me–Ch, Th–Th*–Ch. Th–Gy–Mt. Th–Ap. An. Ap. Le–Sm.	2–3
−175	−150	Me–He–Me*. Me–He–Ap. Me–Ap. Me–He–Th–Le. Me–Th–Ph–Ch. Th*–Ch–Le. Na–Ch. Ch–Sm.	2–3
−150	−125	Me. Me–Th–Ph–Ch. Ph–Sm. Me*–Ch An–Sm.	2–3
−125	−100		
−100	−75	Me. Me–Th–Ch–Sm. Me+Na–Ap–Sm. Me*–Ch. An–Ep–Ch. Mo–Ch. Th–Ch.	2–3
−75	−50	He. He–Th. Mo–He. Me–Th. Na–Ch. Th–Ch. Me*–Ch. Ch–Sm.	3–4
−50	−25	Ch–Sm. Ep–Ch.	3–4
−25	0	Me. Me*. Me–Ap. Me–Th. Me*–Ch. Mo–Ch.	2–3